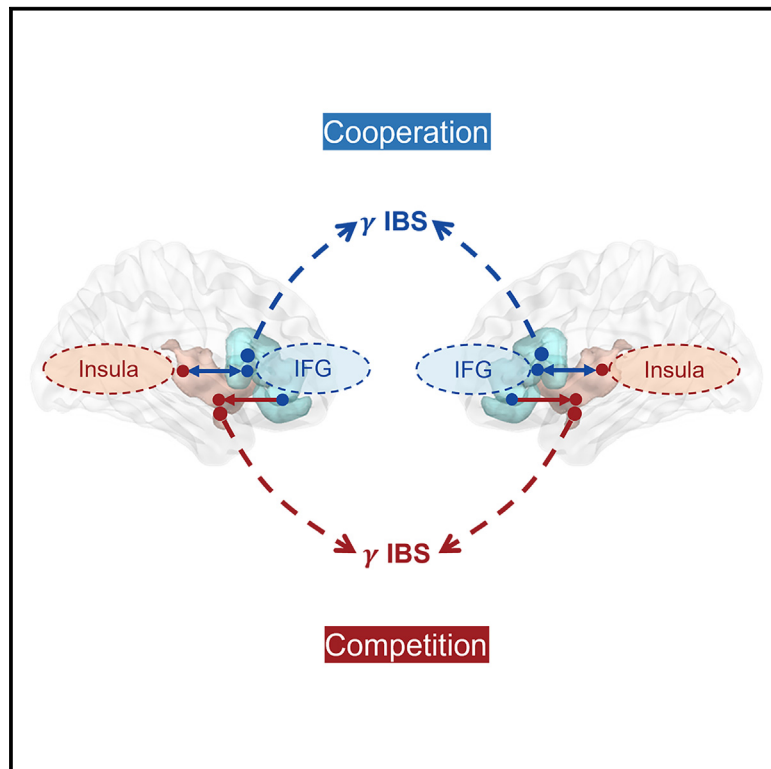


# Exploring the neural mechanisms underlying cooperation and competition behavior: Insights from stereo-electroencephalography hyperscanning

## Graphical abstract



## Authors

Xiaojun Qiao, Rui Li, Huimin Huang, ..., Yongna Xiao, Mingxiang Weng, Junsong Zhang

## Correspondence

zhangjs@xmu.edu.cn

## In brief

Neuroscience; Behavioral neuroscience; Cognitive neuroscience

## Highlights

- High-gamma responses in the insula and IFG are linked to cooperation and competition
- Direct influence from intra-brain IFG to insula during competition
- A more balanced intra-brain IFG-insula interaction during cooperation
- Higher gamma inter-brain synchrony for insula in competition, for IFG in cooperation



## Article

# Exploring the neural mechanisms underlying cooperation and competition behavior: Insights from stereo-electroencephalography hyperscanning

Xiaojun Qiao,<sup>1,2,4</sup> Rui Li,<sup>1,4</sup> Huimin Huang,<sup>1</sup> Yang Hong,<sup>1</sup> Xiaoran Li,<sup>2</sup> Ziyue Li,<sup>2</sup> Siyi Chen,<sup>2</sup> Lizhi Yang,<sup>2</sup> ShengTeng Ong,<sup>2</sup> Yi Yao,<sup>3</sup> Fengpeng Wang,<sup>3</sup> Xiaobin Zhang,<sup>3</sup> Kao-Min Lin,<sup>3</sup> Yongna Xiao,<sup>3</sup> Mingxiang Weng,<sup>3</sup> and Junsong Zhang<sup>2,5,\*</sup>

<sup>1</sup>Brain Cognition and Computing Lab, National Engineering Research Center of Educational Big Data, Central China Normal University, Wuhan, Hubei 430079, China

<sup>2</sup>Brain Cognition and Intelligent Computing Lab, Department of Artificial Intelligence, School of Informatics, Xiamen University, Xiamen, Fujian 361005, China

<sup>3</sup>Epilepsy Center, Xiamen Humanity Hospital, Xiamen Fujian 361006, China

<sup>4</sup>These authors contributed equally

<sup>5</sup>Lead contact

\*Correspondence: zhangjs@xmu.edu.cn

<https://doi.org/10.1016/j.isci.2024.111506>

## SUMMARY

Cooperation and competition are essential social behaviors in human society. This study utilized hyperscanning and stereo-electroencephalography (SEEG) to investigate intra- and inter-brain neural dynamics underlying these behaviors within the insula and inferior frontal gyrus (IFG), regions critical for executive function and mentalizing. We found distinct high-gamma responses and connectivity patterns, with a stronger influence from IFG to insula during competition and more balanced interactions during cooperation. Inter-brain synchronization shows significantly higher insula gamma synchronization during competition and higher IFG gamma synchronization during cooperation. Cross-frequency coupling suggests that these gamma synchronizations result from intra- and inter-brain interactions. Competition stems from intra-brain alpha-gamma coupling from IFG to insula and inter-brain IFG alpha synchronization, while cooperation is driven by intra-brain beta-gamma coupling from insula to IFG and inter-brain insula beta synchronization. Our findings provide insights into the neural basis of cooperation and competition, highlighting the roles of both insula and IFG.

## INTRODUCTION

Humans are social animals that rely on cooperation and competition for survival and development.<sup>1</sup> Cooperation and competition are two different but interrelated modes of social interaction. Both require individuals to monitor their own behavior and those of others, leading to different psychological and behavioral outcomes that contribute to human development.<sup>2</sup> While they differ in focus—cooperation balancing self- and other-monitoring to achieve shared goals, and competition emphasizing self-oriented performance—they are not mutually exclusive. Understanding the cognitive processes and neural bases of cooperation and competition is essential not only for understanding human social behavior but also for improving the lives of individuals with social deficits, such as children with autism spectrum disorder.<sup>3,4</sup> Studies investigating cooperation and competition have consistently revealed their dependence on executive functions and mentalizing abilities.<sup>2,5</sup> Executive function, a higher-order cognitive process that facilitates new behaviors, is associated with various aspects of competitive and cooperative behaviors, such as selecting appropriate actions in different con-

texts, inhibiting inappropriate responses, and monitoring.<sup>6,7</sup> Mentalizing, the ability to understand the thoughts, feelings, and intentions of others, is more strongly linked to cooperative behavior.<sup>8,9</sup> Although many studies have explored the neural activities associated with executive functions and mentalization abilities in social behaviors,<sup>10,11</sup> the underlying neural oscillatory dynamics supporting these interactions have remained unclear.

Previous studies on social interactions have emphasized the critical role of the prefrontal cortex (PFC). Within the PFC, the inferior frontal gyrus (IFG) is particularly important for both cooperative and competitive interactions, as it plays a key role in executive function and mentalization. Evidence from brain damage studies shows that damage to the IFG impairs executive function, such as response inhibition.<sup>12,13</sup> Furthermore, the IFG is a core brain region of the putative mirror neuron system (pMNS), which is involved in social motor information processing and mimicking the behavior of others.<sup>14</sup> The pMNS also facilitates the mentalizing process, especially when biological motion is involved in the interaction.<sup>15,16</sup> The IFG has been shown to be involved in understanding the actions, intentions, and emotions of others.<sup>17,18</sup> Specifically, in cooperative and competitive



interactions, the IFG is essential for coordinating behavior, understanding the perspectives of others, and developing strategies.<sup>19–21</sup> Its functional contributions are closely linked to those of other regions in the mentalizing network, making it a significant area of interest for theoretical exploration.<sup>22–24</sup>

Beyond the IFG, the insular cortex is another key region involved in executive processes, particularly for integrating sensory input and monitoring performance.<sup>25,26</sup> The anterior insula is believed to serve as a central hub for cognitive processing, as it exerts influence over the activity of other brain regions involved in executive control and attention.<sup>27,28</sup> However, research on the insula in the context of social interaction is still in its early stages due to its location and highly vascular anatomy.<sup>29</sup> Despite these challenges, single-brain fMRI studies have shown that the insula is activated during cooperative and competitive interactions. For example, Decety et al. found the activation of the insular cortex in participants engaged in a specially designed computer game for investigating cooperation and competition,<sup>2</sup> while Rilling et al. reported significant anterior insula activation during non-cooperation in the prisoner's dilemma game.<sup>30</sup> These studies provide evidence that the IFG and insula are involved in social interaction at the level of the individual brain. However, social interaction is inherently a two-person (or more) phenomenon. Single-brain studies can identify and characterize brain activity associated with specific social paradigms, but they may not directly access the dynamic interplay and synchronization between two (or more) brains.

The development of hyperscanning technology presents an opportunity to explore social interactions more deeply.<sup>31</sup> Hyperscanning, a technique that allows for the simultaneous recording of brain activity from two or more individuals interacting with each other, offers a valuable tool for investigating the dynamic interactions between individuals.<sup>32</sup> According to mutual prediction theory, inter-brain synchronization (IBS) occurs when individuals with predictive coding capabilities anticipate each other's actions, leading to synchronized neural activity.<sup>33,34</sup> Measuring IBS captures the neural dynamics underlying mutual prediction and coordination, leading to a more comprehensive understanding of social interactions. Hyperscanning studies using fNIRS or EEG have found that the IBS, particularly between frontal regions, is more pronounced during cooperation than during competition or non-cooperation.<sup>35,36</sup> The IFG has been implicated in social alignment<sup>26</sup> and plays a role in both language- and movement-related cooperative and competitive interactions, as evidenced by significant IBS observed in activities such as cooperative singing, synchronized movement, and joint attention.<sup>21,37,38</sup> Meanwhile, due to its deep location in the brain, the insula is often studied with fMRI hyperscanning. For instance, Shaw et al. demonstrated insular activation and synchronization during a modified interactive ultimatum game involving cooperation and competition.<sup>39</sup> Similarly, Xie et al. found bilateral insula activation during collaborative drawing in a triadic fMRI hyperscanning paradigm.<sup>40</sup> Yoshioka et al. revealed task-specific inter-brain neural synchronization within the anterior insular cortex-IFG complex during joint attention tasks.<sup>41</sup>

Although previous studies have explored the role of the insula and IFG in cooperative and competitive interactions, the neural mechanisms of their dynamic intra-brain interactions and inter-brain synchronization within the time-frequency domain remain incomplete. The IFG has reciprocal connections with regions involved in performance monitoring, such as the insula and anterior cingulate cortex, as well as areas involved in higher-order sensory processing, like the temporal and parietal lobes.<sup>26,42</sup> A cortical-cortical evoked potential (CCEP) study demonstrated that the insula and IFG were functionally connected, primarily through ipsilateral pathways, which may be crucial for rapid sensory and executive processing during social interactions such as cooperation and competition.<sup>29</sup> However, the communication dynamics between these regions during such interactions are not yet fully elucidated. Neuronal oscillations, especially phase synchronization, play a key role in facilitating communications between brain regions.<sup>43–45</sup> Exploring the oscillatory interactions between IFG and insula is therefore essential for gaining a deeper understanding of the intra- and inter-brain neural mechanisms underlying social interactions.

Conventional brain recording techniques have limitations in accurately capturing the precise time-frequency activity and inter-brain interaction of deep brain regions. While fMRI offers high spatial resolution, it measures a surrogate signal and is constrained by both physical and biological factors.<sup>46</sup> Scalp-based EEG or fNIRS provide superior temporal resolution compared to fMRI, but their ability to capture deep brain activity is limited.<sup>47</sup> In contrast, stereo-electroencephalography (SEEG) enables high spatial and temporal resolution recordings of neuronal activity within the brain, making it one of the most effective methods for characterizing neural oscillation and dynamic changes across time and regions.<sup>48</sup> However, due to the constraints of the acquisition environment and individual patient characteristics, no previous study has simultaneously recorded SEEG from two patients in two-person games. This underscores the need for a combination of SEEG and hyperscanning to investigate the intricate intra- and inter-brain neurodynamic synchronization during social interactions.

In this study, we aim to combine SEEG and hyperscanning to investigate the intra- and inter-brain interactions of the insula and IFG in cooperation and competition. The environmental setup and experiment paradigm are illustrated in [Figure 1A](#) and detailed in Methods. To induce participants' cooperative or competitive psychological states while minimizing operational discrepancies across different tasks, we employ a modified version of Cui's computer-based task.<sup>35</sup> In the experiment, participants were presented with a target cue and instructed to either cooperate by trying to respond simultaneously or compete by responding as quickly as possible. Real-time feedback was provided following each trial, informing participants of their outcomes (win or loss), scores, and speed, thereby influencing their subsequent responses. Our primary research questions focus on how the insula and IFG synchronize and modulate one another in different social contexts. Specifically, we hypothesize that both cooperation and competition activate the insula and IFG, but with different temporal patterns. For connectivity between the two regions, cooperation will result in more balanced, reciprocal coupling, while

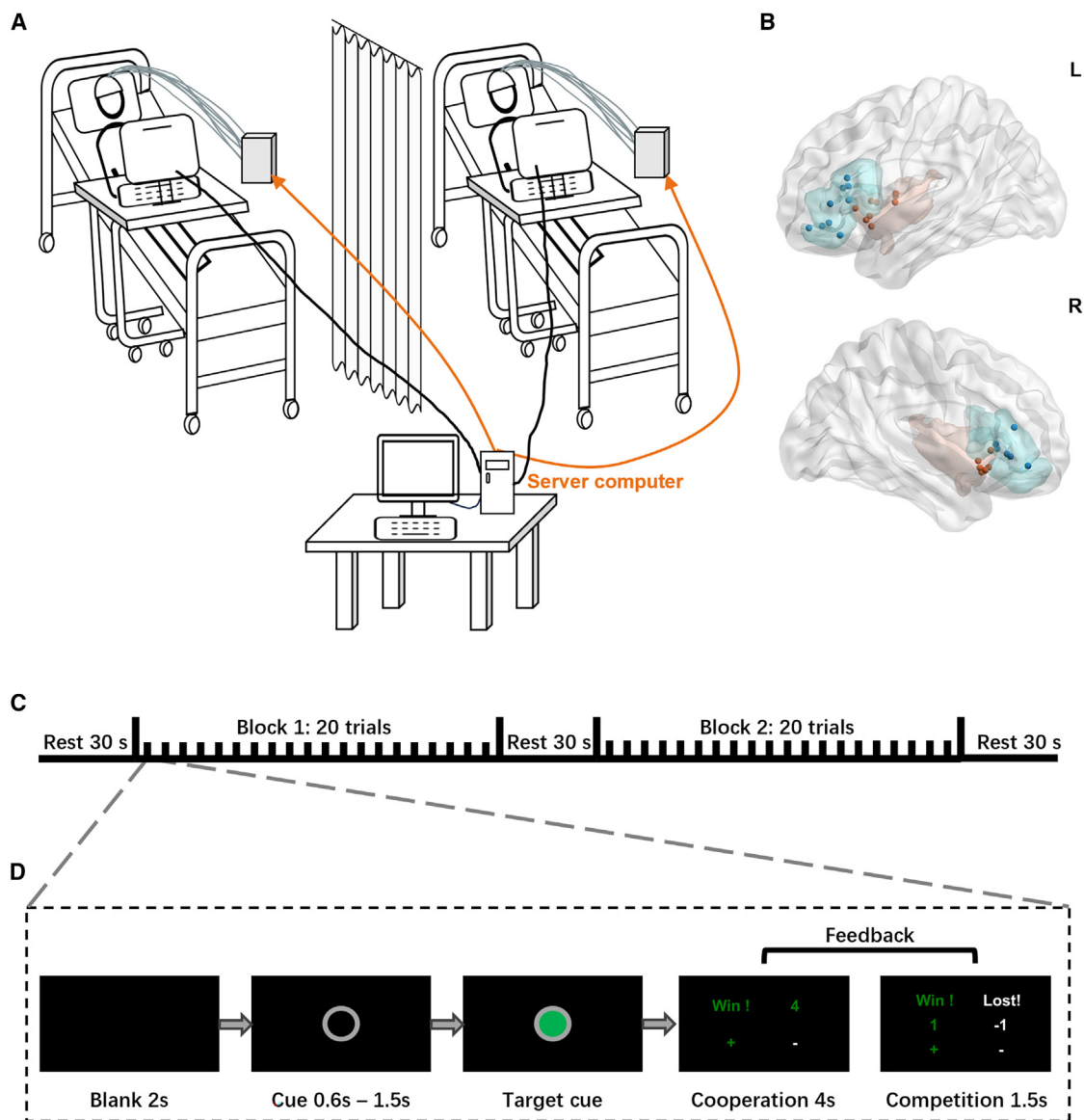


**Figure 1. Experimental setting, task flow, and electrode channel localization**

(A) The experimental setting.

(B) The electrode localization of 15 participants (used for data analysis) was rendered onto a three-dimensional MNI space and visualized using the BrainNet Viewer toolbox ([www.nitrc.org/projects/bnv/](http://www.nitrc.org/projects/bnv/)). Aqua dots indicate electrodes in the inferior frontal gyrus (IFG); orange dots represent electrodes in the insula (L, left; R, right).

(C) Each task consisted of two blocks, with each block comprising 20 trials. Each task in the formal experiment followed Rest 1 (30s), Block 1, Rest 2 (30s), Block 2, and Rest 3 (30s).

(D) In each trial, a blank screen (2 s) was presented first, followed by a cue with a random delay (0.6–1.5 s), then a target cue was presented, participants responded by pressing a button, and then the feedback (cooperation, 4s; competition, 1.5s) was presented.

competition will lead to a stronger, directed influence of IFG on insula activity, given the IFG's role in executive function and mentalizing. Additionally, based on previous hyperscanning studies, we predict higher IBS of IFG and higher IBS of insula during cooperation compared to competition. By leveraging the high spatial and temporal resolution of SIEEG, we aim to gain deeper insights into the specific neural mechanisms underlying IBS during social interactions.

## RESULTS

### Behavioral results

After excluding participants with seizure discharges or epileptogenic zones in the insula or IFG, 15 participants were finally included for individual-level analysis, while 7 pairs of participants were included for group-level analysis. Participant characteristics are provided in [Table 1](#) and [Table S1](#). For each

**Table 1. Patient profile**

Patient ID	Gender	Age	Seizure Onset Age	ROI Electrode Coverage	Seizure Onset	Hemisphere Analyzed	Number of Insula Electrodes	Number of IFG Electrodes
PT001	F	43	10	L, R	Left temporal (medial-lateral)	Left	4	6
PT002	F	33	18	L	Left temporal (medial-lateral)	Left	6	4
PT003	M	56	42	R	Right central parietal	Right	3	4
PT004	M	28	23	R	Right temporal (medial)	Right	12	1
PT005	M	20	17	L	Left temporal (medial)	Left	7	8
PT006	M	26	16	L, R	Right temporal (medial)	Left	3	8
PT007	M	29	12	L, R	Right temporal insula	/	/	/
PT008	F	31	26	L	Left occipital	Left	4	1
PT009	F	16	11	L	Left frontal (medial)	Left	5	4
PT010	F	16	5	L, R	Right central operculum	Left	3	4
PT011	M	28	4	R	Right temporal	Right	9	2
PT012	F	32	16	L, R	Right orbital frontal	Right	4	6
PT013	F	16	12	L	Left temporal-occipital (lateral)	Left	8	4
PT014	M	33	4	L	Left temporal (medial-lateral)	Left	7	4
PT015	M	22	9	L, R	–	Right	7	4
PT016	F	22	9	L, R	Left temporal and insula	Right	7	4

F-female, M-male, L-left, R-right, IFG-Inferior frontal gyrus. Seizure onset refers to the identified location of the epileptogenic zone within the brain, with dashed indicating an undetermined single lesion location.

See also [Table S1](#) and [Table S2](#)

task, we computed the average response time (RT) for the 15 participants and the RT per block. Furthermore, we calculated the difference in response times (RTs) between 7 pairs within the same task, denoted as the difference between the RTs ( $\Delta$ RT) of two participants in the same pair for that task. The overall mean RT of participants was 253.82 ms ( $SEM = 4.13$ ) in competitive interaction and 565.25 ms ( $SEM = 29.76$ ) in cooperation. The Wilcoxon rank-sum test (also known as the Mann-Whitney U test) showed that the dyads responded significantly faster in competition than in cooperation ( $Z = -9.056$ ,  $p < 0.001$ , two-sided) (Figure 2C). No significant differences in RTs were observed between the two blocks within the same task, as assessed by Wilcoxon rank-sum tests (Figure S1A; competition:  $Z = -0.463$ ,  $p = 0.634$ , cooperation:  $Z = -0.174$ ,  $p = 0.862$ , two-sided). Additionally, we found that the difference between the button responses of dyads ( $\Delta$ RT) during the competition (mean  $\Delta$ RT = 79.71 ms,  $SEM = 6.12$ ) was smaller than that during cooperation (mean  $\Delta$ RT = 154.36 ms,  $SEM = 14.02$ ) ( $Z = -2.464$ ,  $p = 0.014$ , two-sided). The overall percentage of winning trials (PWT) during cooperation was 58%. No significant difference in PWT was observed between the two blocks (Figure S1B;  $p = 0.235$ , two-sided). Similarly, no significant differences were found in difference of response time (Figure S1C;  $p = 0.117$ , two-sided), brain activities (Figure S1D;  $p = 0.738$  for insula,  $p = 0.703$  for IFG, two-sided), or inter-brain synchronization across the two blocks (Figure S1E;  $p = 1$  for insula,  $p = 1$  for IFG, cluster-based permutation test), suggesting that participants' performance did not change significantly over time in this study. Given the mean RTs for the cooperation and competition tasks, the

main time windows of interest for subsequent intra-brain analyses were 0–300 ms for competition and 0–600 ms for cooperation.

### Distinct time-frequency activity patterns of the insula and inferior frontal gyrus in cooperation and competition

To compare the neural activities of the insula and IFG in cooperative and competitive interactions, we performed a time-frequency analysis across the entire frequency spectrum (1–140 Hz). Consistent with previous literature, we focused on high-gamma frequency activity (70–140 Hz) using high-frequency broadband amplitude (HFBA) as a specific measure (see STAR Methods). The results of the time-frequency analysis showed that during competitive interactions, the insula exhibited sustained oscillatory activity in the delta and theta bands (~1–7 Hz) after target onset (0 ms), and the beta, low-gamma, and middle-gamma bands (~20–70 Hz) after 300ms, while IFG exhibited sustained oscillatory activity in the delta, theta, alpha, and beta bands (~1–20 Hz) after target onset (Figure 2A left). In contrast, cooperation displayed a sequential activation pattern: the IFG exhibited strong oscillatory activity in the theta, alpha, and beta bands (~4–20 Hz) within 300 ms after the appearance of the cooperative target cue, followed by a decline, while the insula showed increased activity after 300 ms in the delta, theta, and alpha bands (~3–10 Hz), as well as the beta, low-gamma and middle-gamma band range (~20–70 Hz) (Figure 2A right). In competition, both the insula and IFG exhibited sustained oscillatory activity across multiple frequency bands after target onset, suggesting a sustained state of neural activation. Cooperation,

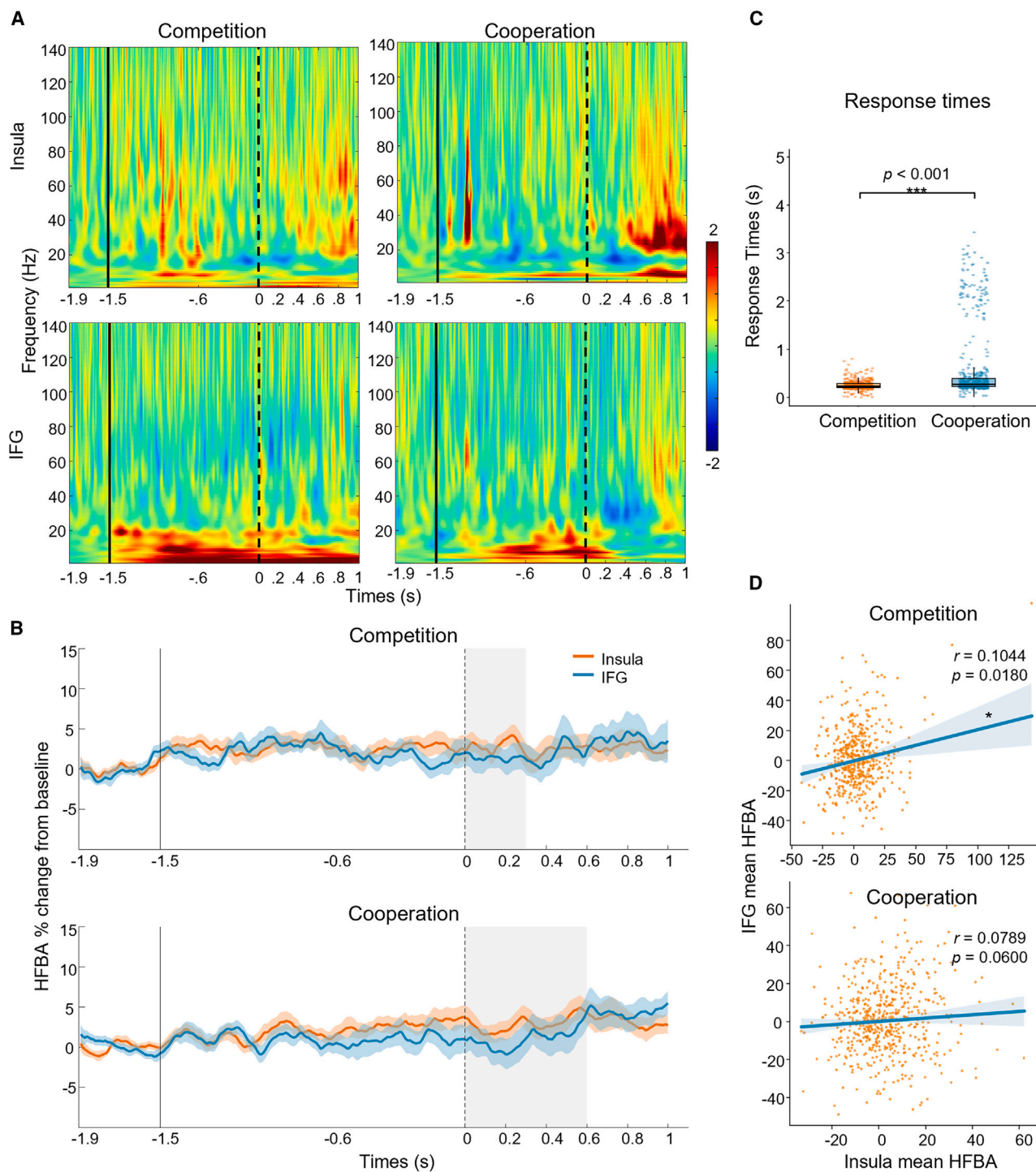


**Figure 2. Task-related low-frequency and high-frequency activities, and behavioral results**

(A) Averaged power of electrodes in the insula (top) and the IFG (bottom) across all 15 subjects, normalized to the baseline period (-1900ms ~ -1500ms) and grouped according to tasks (competition on the left; cooperation on the right). Warmer colors denote task-induced power increases from the baseline, while cooler colors refer to power decreases from the baseline. Vertical black dashed lines indicate the target cue onsets. The period before the vertical black solid lines represents the baseline.

(B) Task-related responses were quantified through high-frequency activity. High-frequency broadband amplitude (HFBA) quantified high-frequency activities were averaged for the insula (orange) and IFG (aqua) across all subjects. Gray rectangular shaded areas represent the periods of interest for the competition (top,

(legend continued on next page)

however, was characterized by sequential activation, with IFG initially activating first, followed by the insula.

High-gamma frequency activity (HFA), considered a critical analytical signal in human intracranial recordings, is generally believed to reflect local neural firing.<sup>49</sup> It is closely associated with neuronal spikes<sup>50,51</sup> and has been demonstrated to exhibit correlations with blood-oxygen-level-dependent (BOLD) signals in fMRI studies.<sup>52,53</sup> The HFA was quantified using HFBA, and the results showed that in competitive interactions, both the insula and IFG showed an upward trend (Figure 2B top). While in cooperation, HFBA in both regions initially decreased and then increased (Figure 2B bottom). The mean responses of the two brain regions were significantly correlated across trials during competition (0–300 ms) (Spearman correlation,  $r = 0.1044$ ,  $p = 0.018$ ) (Figure 2D top), but no significant correlation was found during cooperation (0–600 ms) (Spearman correlation,  $r = 0.0789$ ,  $p = 0.060$ ) (Figure 2D bottom). Further analysis of the 0–300 ms interval during cooperation also showed no significant correlation (Spearman correlation,  $r = 0.0525$ ,  $p = 0.210$ ). A comparison of HFBA revealed no significant lateralization effects in the insula and IFG within the current data (Cooperation:  $p_{IFG} = 0.7135$ ,  $p_{insula} = 0.1903$ ; Competition:  $p_{IFG} = 0.4634$ ,  $p_{insula} = 0.3892$ ; see Table S5). In summary, competition was associated with sustained oscillatory activity and significant positive HFBA correlations between the insula and IFG, suggesting continuous neural engagement. In contrast, cooperation followed a sequential activation pattern, with no significant HFBA correlation observed between the two regions.

### Low-frequency insula-inferior frontal gyrus synchrony supports intra-brain competition and cooperation

To obtain the synchronized connectivity between the insula and IFG during tasks, we examined phase synchronization between these regions across the 1–140 Hz range using the weighted phase lag index (wPLI, see STAR Methods), which helps reduce noise and volume conduction effects.<sup>54</sup> The cluster-based permutation test results revealed different synchronization patterns between tasks. Specifically, competition exhibited synchronization within the sub-40 Hz frequency range during the 0–300 ms time window (Figure 3A top), while cooperation showed synchronization in the delta (~2–4 Hz) and beta (~20–30 Hz) bands during the 0–600 ms time window (Figure 3A bottom). To validate the band specificity of insula-IFG synchronization, we compared wPLI values between competition (0–300 ms) and cooperation (0–600 ms) using the Wilcoxon rank-sum test (see STAR Methods and Table S4). The results indicated significantly higher synchronization in the beta and high-gamma bands during cooperation compared to competition (beta:  $p = 0.0207$ , high-gamma:  $p = 0.0173$ , two-sided), while other frequency bands (delta, theta, alpha, low-gamma, middle-gamma) showed higher synchroniza-

tion during the competition ( $p < 0.001$ , two-sided). The neural synchronization was higher for competition compared to cooperation, which might be due to increased cortical activity and inter-regional connectivity to accommodate the heightened processing demands of competitive tasks.<sup>55</sup>

To investigate the nonlinear interactions between oscillatory frequencies across the insula and IFG, we measured the high-to-low cross-frequency coupling (CFC) using envelope-to-signal coupling (ESC, see STAR Methods). ESC has been found to be effective in revealing interregional interactions associated with specific tasks and events.<sup>56</sup> We computed cross-regional ESC between the 1–30 Hz signal from the insula and the 30–140 Hz envelope from the IFG, and vice versa. The results showed frequency-specific features under different tasks. As illustrated in Figure 3C left, in competition, theta and alpha (~4–10 Hz) oscillations from the insula modulated low-gamma (~30–40 Hz), middle-gamma and high-gamma (~60–80 Hz, ~110–140 Hz) activities in the IFG. In turn, delta (~1–4 Hz) oscillations from the IFG modulated low-gamma (~30–45 Hz), middle-gamma, and high-gamma (~55–80 Hz) activities of the insula, while theta and alpha (~7–9 Hz) oscillations from the IFG modulated middle-gamma (~50–65 Hz) activities of the insula. In contrast, during the cooperation (Figure 3C right), we found that delta (~1–3 Hz) oscillations from the insula modulated low-gamma (~30–35 Hz) and high-gamma (~80–90 Hz) activities in the IFG, theta, and alpha (~5–9 Hz) oscillations from the insula modulated low-gamma and middle-gamma (~30–70 Hz) activities in the IFG, and beta (~13–16 Hz and 25–29 Hz) oscillations from the insula modulated middle-gamma (~50–60 Hz) and high-gamma (~90–95 Hz) activities in the IFG. Additionally, delta and theta (~3–5 Hz) oscillations from the IFG modulated low-gamma (~30–40 Hz) activities in the insula, and alpha (~8–12 Hz) and beta (~13–17 Hz) oscillations from the IFG modulated the high-gamma (~80–100 Hz, 120–140 Hz) activities of the insula. In summary, bidirectional low-to-high CFC between the insula and IFG was observed during both cooperation and competition interactions, with competition primarily engaging 1–10 Hz oscillations and cooperation involving additional beta oscillations above 13 Hz.

To further test whether the insula and IFG work independently or interact with each other in competitive and cooperative tasks, we investigated the directionality of information flow between the insula and IFG using the phase slope index (PSI, see STAR Methods).<sup>57</sup> PSI measures the phase difference between two signals as a function of frequency. A positive phase slope indicates that the signal from the first region leads to the signal from the second region. Guided by the intra-brain wPLI findings that revealed significant phase synchronization bands within the sub-40 Hz range, we selected the 1–40 Hz range for PSI analysis. Our results showed that the IFG drives the insula almost exclusively during competition ( $z < -1.96$ ,  $p < 0.05$ ) (Figure 3B top).

0–300ms) and cooperation (bottom, 0–600ms) tasks. Vertical black dashed lines indicate the onsets of the target cue. The period before the vertical black solid lines is the baseline. The orange and aqua shaded areas represent the SEM.

(C) Response times of 15 subjects are displayed on the y axis in seconds. The boxplots indicate the median (horizontal line inside the box), the interquartile range (height of the box), and the total range excluding outliers (whiskers). The Wilcoxon rank-sum test showed that response time was significantly faster in the competition than in the cooperation ( $p < 0.001$ ).

(D) Correlation analysis between the mean HFBA in the insula (x axis) and IFG (y axis) of each participant, on a trial-by-trial basis (Competition, top,  $r = 0.1044$ ,  $p = 0.0180$ ; Cooperation, bottom,  $r = 0.0789$ ,  $p = 0.0600$ ). The aqua shaded areas represent the 95% confidence.

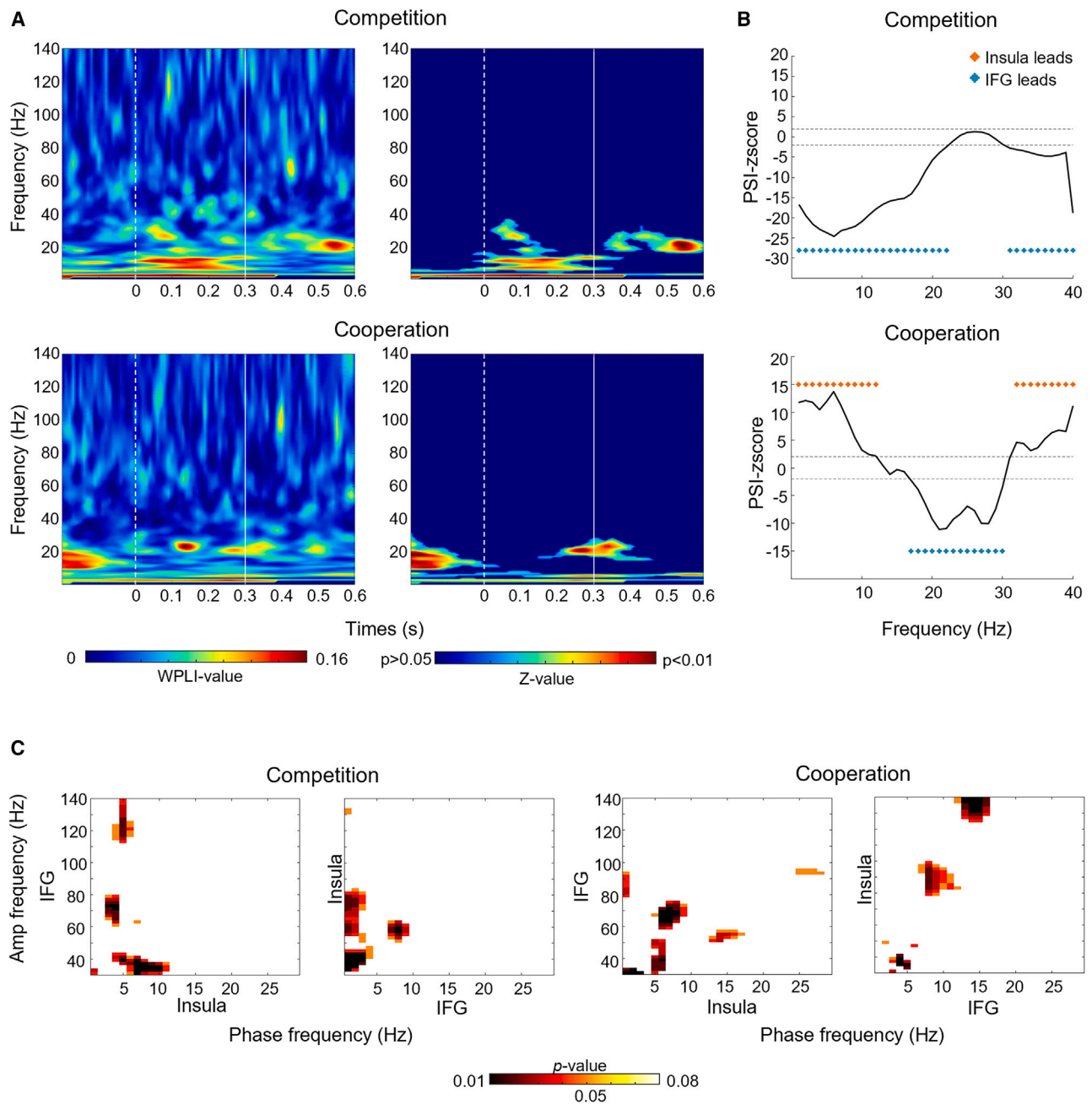


**Figure 3. Different insula-IFG interaction patterns in cooperation and competition**

(A) Averaged insula-IFG synchrony for 15 participants during the competition (top) and cooperation (bottom) tasks. The synchronization is quantified by the weighted phase lag index (wPLI) (the left panel of each task). The color scale indicates the synchronization level, with warmer colors denoting higher wPLI values, thus greater synchronization. The right panels display statistical significance ( $p < 0.05$ ) obtained from a cluster-based permutation test comparing observed wPLIs to null distributions, with warmer colors indicating lower  $p$  values. Dashed vertical lines at time 0 represent the onset of the target cue. Vertical solid lines at time 300 indicate the 300 ms post-onset.

(B) Averaged z-scored phase slope index (PSI) for 15 participants across 1–40 Hz during competition (top) and cooperation (bottom). Orange asterisks indicate significant PSI from the insula to the IFG, aqua asterisks indicate the opposite direction (statistical significance threshold as  $|z| > 1.96$ ).

(C) Averaged intra-brain envelope-to-signal coupling (ESC) within insula-IFG for 15 participants in the competition (left) and cooperation (right) tasks. Warmer colors indicate lower  $p$  values (permutation test,  $p < 0.05$ ).

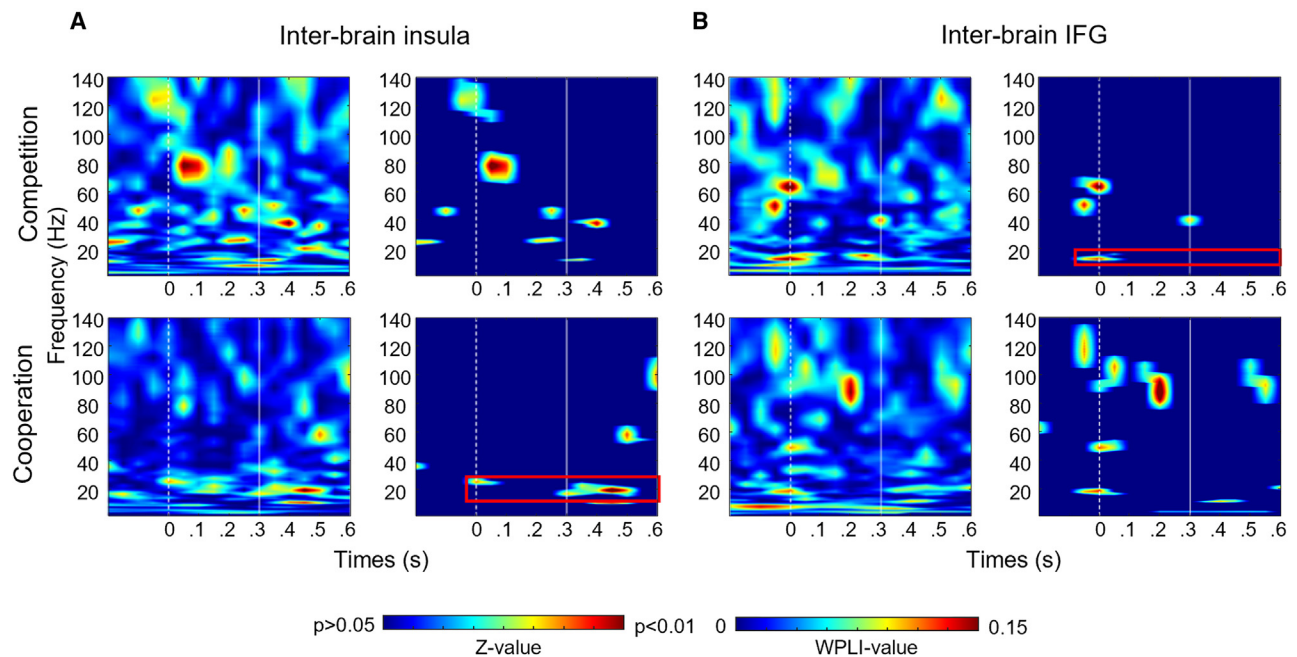


**Figure 4. Inter-brain synchronization in insula and IFG during competition and cooperation tasks**

(A) Averaged weighted phase lag index (wPLI) of inter-brain insula for 7 dyads during competition (top) and cooperation (bottom) tasks. The left graphs represent the wPLI values across a frequency range (y axis) over the task duration (x axis), with the color intensity reflecting the degree of phase synchronization; warmer colors indicate higher wPLI values. The right graphs depict the statistical significance of these wPLI values, with warmer colors denoting regions where phase synchronization significantly exceeds null distributions of the cluster-based permutation test ( $p < 0.05$ ). The red line rectangular box highlights the potential contributions of inter-brain insula beta synchronization to inter-brain IFG gamma bands synchronization during cooperation. The vertical dashed lines at 0 s indicate the onset of the target cue. Vertical solid lines indicate the 300 ms post-onset.

(B) Averaged wPLI of inter-brain IFG for 7 dyads during competition (top) and cooperation (bottom) tasks. The red line rectangular box highlights the potential contributions of inter-brain IFG alpha synchronization to inter-brain insula gamma bands synchronization during competition.

During the cooperation, there were unidirectional insula-to-IFG connections at 1–12 Hz ( $z > 1.96$ ,  $p < 0.05$ ), and IFG-to-insula connections at 17–30 Hz ( $z < -1.96$ ,  $p < 0.05$ ) (Figure 3B bottom). Spectral Granger causality (spectral GC) analysis further confirmed these findings, showing a stronger influence from IFG to insula during competition and more balanced bidirectional causality during cooperation (see STAR Methods and Figure S2). Together, these results suggest distinct frequency-specific directional connections between the two regions during these tasks, with competition primarily driven by the IFG and cooperation characterized by bidirectional interactions.

### Inter-brain synchrony

Inter-brain synchronization within dyads was quantified using wPLI across a frequency range of 1–140 Hz. The results revealed distinct frequency-specific inter-brain synchrony patterns in the insula and IFG during cooperation and competition. For inter-brain insula interactions, significant synchronization was observed in beta (~20–30 Hz), low-gamma (~40–50 Hz), and high-gamma (~70–90 Hz, 110–140 Hz) bands before 300 ms when the dyads competed (cluster-based permutation test) (see STAR Methods and Figure 4A top). In contrast, when the dyads cooperated with each other, synchronization in theta and alpha (~9–11 Hz), beta (~18–30 Hz), and middle-gamma bands (~50–70 Hz) was observed during the 0–600 ms period

(Figure 4A bottom). For inter-brain IFG interactions, competition exhibiting significant synchronization in the alpha (~9–13 Hz), low-gamma (~35–45 Hz), and middle-gamma (~55–70 Hz) bands before 300 ms (Figure 4B top). In cooperation, significant synchronization occurred in the theta (~4–5 Hz), alpha (~10–12 Hz), beta (~15–20 Hz), middle-gamma (~48–55 Hz), and high-gamma (~80–110 Hz) bands during the 0–600 ms (Figure 4B bottom). The time windows for inter-brain synchronization differed between tasks, with cooperation showing synchronization throughout the 0–600 ms window and competition primarily within the 0–300 ms window.

In this study, we conducted a detailed comparison of inter-brain synchronization during competitive (0–300 ms) and cooperative (0–600 ms) tasks to determine significant differences across various frequency bands. Using the Wilcoxon rank-sum test, we identified significant inter-brain wPLI differences, revealing task-dependent synchrony patterns (as detailed in Tables 2 and 3). Specifically, for inter-brain insula synchronization, competition was associated with higher median wPLI values in the theta, alpha, low-gamma, middle-gamma, and high-gamma bands ( $p = 0.0074$ ,  $p = 0.0297$ ,  $p < 0.001$ ,  $p < 0.001$  and  $p < 0.001$ , respectively, two-sided), while cooperation exhibited higher wPLI values in the beta band ( $p < 0.001$ , two-sided). In the inter-brain IFG synchronization, a distinct pattern was observed: competition showed higher wPLI values in the middle-gamma

**Table 2. Comparison of inter-brain insula median wPLI values under two tasks and statistical significance of differences**

Bands	Competition	Cooperation	Significance ( $p$ -value)
Delta	0.0366	0.0444	0.1623
Theta	<b>0.0320</b> **	0.0201	0.0074
Alpha	<b>0.0362</b> *	0.0207	0.0297
Beta	0.0294	<b>0.0460</b> ***	<0.001
Low-gamma	<b>0.0310</b> ***	0.0206	<0.001
Middle-gamma	<b>0.0408</b> ***	0.0215	<0.001
High-gamma	<b>0.0350</b> ***	0.0247	<0.001
1-140 Hz	<b>0.0354</b> ***	0.0255	<0.001

band ( $p = 0.0031$ , two-sided), while cooperation had higher wPLI values in the delta, low-gamma, and high-gamma bands ( $p = 0.0015$ ,  $p < 0.001$  and  $p = 0.0020$ , respectively, two-sided). No significant differences were detected in the theta, alpha, and beta bands between the task conditions ( $p = 0.9062$ ,  $p = 0.1503$ , and  $p = 0.7044$ , respectively, two-sided). Notably, our findings indicate increased inter-brain insula synchronization in the high-gamma band during competition, while cooperation showed enhanced inter-brain IFG synchronization in the same band. We further investigated task-related differences in inter-brain insula and inter-brain IFG synchronization across the 1–140 Hz frequency range. The results showed that inter-brain insula synchronization was significantly higher during competition across 1–140 Hz (Wilcoxon test,  $competition_{median\ wPLI} = 0.0354$ ,  $cooperation_{median\ wPLI} = 0.0255$ ,  $p < 0.001$ , two-sided), whereas inter-brain IFG synchronization exhibited a higher tendency during cooperative tasks (Wilcoxon test,  $competition_{median\ wPLI} = 0.0252$ ,  $cooperation_{median\ wPLI} = 0.0283$ ,  $p = 0.0662$ , two-sided). Overall, our findings suggest that competition elicits higher IBS of the insula, while cooperation is associated with enhanced IBS of IFG.

## DISCUSSION

The present study, combining SEEG and hyperscanning technology, aims to explore the intra- and inter-brain neural mechanisms of cooperation and competition behavior in a computer game-based paradigm. This experimental design allowed us to simultaneously evaluate the psychological state differences between cooperation and competition with minimal motor differences. Although the importance of intra- and inter-brain coupling for social function has been recognized and explored,<sup>37,58,59</sup> existing studies have rarely revealed the dynamic contributions of deep brain regions due to technical limitations. Our findings provide insights into the neural dynamics of intra- and inter-brain interactions during cooperation and competition, emphasizing the roles of the insula and IFG. We found temporal and spectral variations in oscillation patterns between the insula and IFG, supporting the distinct behaviors between cooperation and competition. More specifically, the two brain regions exhibited different correlations in HFBA, with a significant positive correlation during competition and no significant correlation during cooperation. Additionally, high-gamma frequency activity (HFA)

(70–140 Hz) in the two brain regions was driven by different low-frequency signals. During the competition, unidirectional theta oscillations from the insula enhanced HFA in the IFG, while unidirectional delta oscillations from the IFG enhanced HFA in the insula. In cooperation, HFA activity in the IFG was unidirectionally enhanced by delta, theta, and beta oscillations from the insula, while alpha and beta oscillations from the IFG unidirectionally enhanced HFA activity in the insula. Crucially, our IBS results not only elucidate the influence of cooperation and competition on neural synchronization but also reveal frequency-specific differences, including high-gamma insula synchrony in competition and high-gamma IFG synchrony in cooperation.

At the individual brain level, we found that both cooperation and competition tasks activated the insula and IFG. The insula (especially the anterior insula) and IFG are both part of the salience network, which is activated in response to salient stimuli during tasks with high cognitive demands.<sup>60,61</sup> The insula is involved in sensory input, receiving input from different sensory modalities<sup>25</sup> and integrating bottom-up information to initiate attention control signals.<sup>62</sup> In the present study, participants needed to maintain attention to complete the button-pressing task, whether cooperating or competing. This required integrating sensory input from their own bodies and the environment, leading to the activation of the insula. The IFG, involved in top-down control<sup>63</sup> and the pMNS,<sup>64</sup> plays a crucial role in the motor representation of actions<sup>65</sup> and interpersonal synchronization by regulating the gap between self and others' actions.<sup>26</sup> In our study, during competition, participants focused on reacting quickly to stimuli, leading to strong coordination between sensory input and motor response, which was reflected in the positive correlation between IFG and insula activity (Figure 2D top). In contrast, during cooperation, participants focused more on their partners, which reduced the direct coordination between the two brain regions, resulting in no significant linear relationship between them (Figure 2D bottom). Behaviorally, we observed faster RTs during competition, consistent with previous findings indicating that competition tends to increase response speed as individuals are goal-oriented and strive to outperform their opponents.<sup>35,66</sup>

In addition to observing differences in the activity of the two brain regions, our study identified variations in their phase synchronization across different tasks. Phase synchronization involves the adjustment and maintenance of phase relationships between oscillating neural populations, serving as a mechanism through which oscillations facilitate communication between these neural populations.<sup>67,68</sup> According to our findings on the Wilcoxon test of wPLI within the brain, it appears that competitive tasks prompt a more pronounced intra-brain synchronization between insula and IFG compared to cooperative tasks, except in beta and high-gamma bands, where cooperation shows higher synchronization. Here, we focused on lower frequency interactions between the insula and IFG, given the significance of low-frequency oscillations in facilitating interregional communication.<sup>44</sup> Competition exhibited greater intra-brain synchronization in delta, theta, and alpha bands. During competitive tasks, participants focused more on self-reference, rapidly integrating perceptual information to achieve task goals, leading

**Table 3. Comparison of inter-brain IFG median wPLI values under two tasks and statistical significance of differences**

Bands	Competition	Cooperation	Significance (p-value)
<b>Delta</b>	0.0322	<b>0.0730</b> **	0.0015
<b>Theta</b>	0.0400	0.0397	0.9062
<b>Alpha</b>	0.0354	0.0336	0.1503
<b>Beta</b>	0.0209	0.0237	0.7044
<b>Low-gamma</b>	0.0175	<b>0.0309</b> ***	<0.001
<b>Middle-gamma</b>	<b>0.0269</b> **	0.0202	0.0031
<b>High-gamma</b>	0.0257	<b>0.0296</b> **	0.0020
<b>1-140 Hz</b>	0.0252	<b>0.0283</b>	0.0662

to enhanced intra-brain connectivity. This finding aligns with our time-frequency and HFBA analysis results, indicating a positive correlation between activity in the two brain regions during competition. In contrast, cooperative tasks required participants to additionally integrate information from their partner to achieve a shared goal of aligning response times, contributing to lower levels of intra-brain connectivity compared to competition. Our ESC results revealed that gamma activities (including low-gamma, middle-gamma, and high-gamma) in the insula and IFG in both cooperation and competition predominantly originated from the coupling between lower frequency signals (delta, theta, alpha, and beta) and gamma activities. Notably, the specific low-frequency oscillations involved in this coupling differed between the two tasks. Specifically, delta, theta, and alpha signals were primarily coupled with gamma activities in competition, while beta oscillations were additionally coupled with gamma activities during cooperation. These findings elucidate our intra-brain wPLI results, which demonstrated higher delta, theta, and alpha synchronization during competition and higher beta synchronization during cooperation.

To examine the directionality of the driving effect between the insula and IFG in social interaction across different frequency bands, we performed a PSI analysis. In competition tasks, we observed unidirectional dominance of the IFG over the insula across nearly all frequency bands (1–40 Hz). In contrast, during cooperation tasks, the connectivity between the insula and IFG was more balanced and bidirectional. The IFG, which is involved in top-down attentional control,<sup>63,69</sup> and the insula, which is involved in sensory input and performance monitoring,<sup>25,26</sup> play different roles during competitive and cooperative interactions. In competition, participants may exhibit a greater focus on self-related information, leading to top-down influences of the IFG on the insula. Conversely, during cooperation, participants need to attend to both their own and others' behaviors and performances, resulting in a more balanced relationship between these two regions. Complementary spectral Granger causality (spectral GC) analysis further corroborated the PSI results regarding the directionality of information flow between the insula and IFG.

In this study, we employed hyperscanning technology to measure the brain activities of two participants simultaneously, allowing us to quantify the dyadic interactions during cooperation and competition. Using wPLI, we assessed IBS between the dyads. To ensure consistency, we applied the same wPLI

method to both intra- and inter-brain data. However, the interpretation of the results is context-dependent. For intra-brain connectivity, we focused on understanding how neural oscillations within the insula and IFG interact during cooperative and competitive tasks. For inter-brain connectivity, we examined how these oscillations synchronize between participants during the same tasks. The inter-brain wPLI results revealed a more complex picture than our originally hypothesized, with distinct patterns of synchronization emerging in the two brain regions. Specifically, the Wilcoxon test showed that competition led to higher inter-brain insula synchronization, while cooperation resulted in higher inter-brain IFG synchronization. These findings suggest distinct neural patterns for cooperation and competition. In competition, increased insula synchronization likely reflects participants' heightened focus on external stimuli to accelerate their responses. This synchronization, driven by concurrent sensory inputs,<sup>25</sup> highlights the role of the insula in processing shared environmental stimuli. In contrast, during cooperation, the IFG, part of the pMNS,<sup>64</sup> was more synchronized as participants coordinated their actions, aiming to match each other's button-press speed. This phenomenon transcends mere shared inputs and actions, evidenced by significantly reduced  $\Delta$ RTs between participants during competition, aligning with findings from previous studies.<sup>35,66</sup>

Our cluster-based permutation tests revealed that the IBS, including inter-brain insula and inter-brain IFG, exhibits significant differences in the time windows and frequency bands between the two tasks. We found that IBS patterns aligned with our primary time windows of interest: IBS during cooperation was observed throughout the 0–600 ms, while IBS during competition was primarily evident within the 0–300 ms window. Specifically, during cooperation, inter-brain insula synchronization was predominantly observed after 300 ms, which coincides with enhanced insula activation within the same time frame, as revealed by our time-frequency analysis. For the competition, both the insula and IFG synchronization were mainly observed within the 0–300 ms, with IBS of IFG occurring particularly around the onset (0 ms). We also noted IBS of insula beyond 300 ms, but detailed analyses were not conducted for the post-300ms period due to our primary interest in the response phase and the lack of corresponding IFG synchronization. We speculate that this later insula synchronization may be related to subsequent shared visual input.

Inter-brain synchronization in gamma bands (including low-gamma, middle-gamma, and high-gamma) has garnered significant interest in hyperscanning studies. In our study, we observed higher inter-brain insula gamma synchronization (across low-, middle-, and high-gamma) during competition, while higher inter-brain IFG gamma (specifically in low- and high-gamma) synchronization during cooperation. These results partially diverge from previous research findings. Existing EEG hyperscanning study has identified gamma activity, particularly in the low-gamma range, as an electrophysiological marker of shared intentionality, with enhanced synchronization typically observed during cooperation.<sup>66</sup> Additionally, EEG studies on individuals have linked gamma synchronization with empathy,<sup>70,71</sup> prosocial behavior,<sup>72</sup> and mentalization,<sup>73</sup> consistently underlining the role of gamma synchronization in

**Table 4. Summary of neural activity patterns in cooperation and competition**

	Methods	Key Observations	
		Competition	Cooperation
<b>Intra-brain</b>	Time-frequency	Continuous activation of insula and IFG.	Sequential activation from IFG to insula.
	HFBA	A significant positive correlation in HFBA between the insula and IFG.	No significant correlation in HFBA between the insula and IFG.
	wPLI	Higher $\delta$ , $\theta$ , $\alpha$ , low $-\gamma$ and middle $-\gamma$ synchronization compared to cooperation.	Higher $\beta$ and high $-\gamma$ synchronization compared to competition.
	PSI and GC	IFG $\rightarrow$ insula	IFG $\leftrightarrow$ insula
	CFC	IFG $\leftrightarrow$ insula: modulation of high-frequency amplitude with low-frequency signals below 10 Hz.	IFG $\leftrightarrow$ insula: modulation of high-frequency amplitude with low-frequency signals below 20 Hz.
<b>Inter-brain</b>	wPLI	Higher insula IBS compared to cooperation.	Higher IFG IBS compared to competition.

facilitating cooperative interactions. These findings align with our results for IBS of IFG located in the lateral cortex but differ from our findings for the insula in the medial cortex. This discrepancy may be due to the spatial resolution limitations of scalp EEG, which struggles to capture activity in deeper brain regions such as the insula accurately. Our study underscores the enhanced inter-brain gamma synchronization within the insula during competitive tasks, potentially reflective of the insula's distinctive function in the context of our specific tasks. In summary, these differences highlight the need for further exploration into how task-specific demands influence neural connectivity. Our findings suggest that the role of gamma synchronization in interpersonal interactions may be more complex and context-dependent than previously understood.

The present study provides evidence for distinct intra-brain and inter-brain neural interactions and synchronization patterns within the insula-IFG circuit during competitive and cooperative behavior (as detailed in Table 4). Intra-brain analyses revealed that the IFG primarily influenced the insula within the 1–40 Hz frequency bands during competitive tasks, whereas cooperative tasks facilitated bidirectional interactions between the insula and IFG. Additionally, CFC between lower frequencies and gamma activity was observed within both regions. At the inter-brain level, competition was associated with enhanced gamma synchronization in the insula of dyads, while cooperation promoted greater IFG gamma synchronization. These results align with the theoretical model proposed by Moreau et al., who suggested that inter-brain gamma synchronization can arise from lower-frequency inter-brain coupling and intra-brain CFC.<sup>74</sup> Our SEEG-based hyperscanning data provides real-world evidence supporting this mechanism, showing that during the competition, inter-brain gamma IBS in the insula may stem from inter-brain alpha synchronization in the IFG, coupled with alpha-gamma interactions from IFG to insula. In contrast, during cooperation, inter-brain gamma IBS in the IFG appeared to be driven by inter-brain beta synchronization in the insula, along with beta-gamma coupling from the insula to IFG (see Figure 5).

These findings highlight the distinct neural mechanisms underlying competition and cooperation. During competition, participants focus on quick reactions to stimuli, leading to enhanced

insula synchronization, reflecting shared attention to sensory inputs. Conversely, cooperation demands the synchronization of behavior and mentalizing processes, leading to increased IFG synchronization, a region associated with understanding others' actions. In summary, our SEEG recordings revealed the association between intra-brain neural oscillations and inter-brain neural synchronization. Our study expands the scope of hyperscanning research, which has traditionally focused on the prefrontal cortex,<sup>35,75,76</sup> by exploring deeper brain regions essential to social interactions, such as the insula. Additionally, we provide objective time-frequency evidence for the transition from intra-brain to inter-brain synchronization during social interactions. This study suggests that inter-brain gamma synchronization mechanisms differ between cooperative and competitive contexts and that these differences may be linked to specific frequency couplings between brain regions.

In conclusion, our results provide insights into the electrophysiological mechanisms of insula and IFG involvement in social interactions, offering a reference for more precise time-frequency activity measurement and understanding in this context. These insights contribute to a broader understanding of social cognition and may inform future research on adaptive neural processes in social interactions.

#### Limitations of the study

Our study has some limitations that should be considered. First, this study was conducted on patients with epilepsy, so we cannot exclude the inherent effects of epilepsy. However, we evaluated the participants with the Montreal Cognitive Assessment (MoCA), which should greatly reduce the influence of epilepsy. Following the recommendations of previous research<sup>77</sup> and a comprehensive review of the intracranial study,<sup>78</sup> we excluded data recordings from epileptogenic tissues and surgical areas. While these steps aimed to minimize the influence of epilepsy, the study population consisting entirely of patients with epilepsy introduces potential confounds related to the underlying pathology. Future research should involve a larger, more diverse participant pool to confirm these preliminary results. Second, the study is limited by the small number of patients. Due to the matching requirements and brain region restrictions, the number of patients who met all the conditions

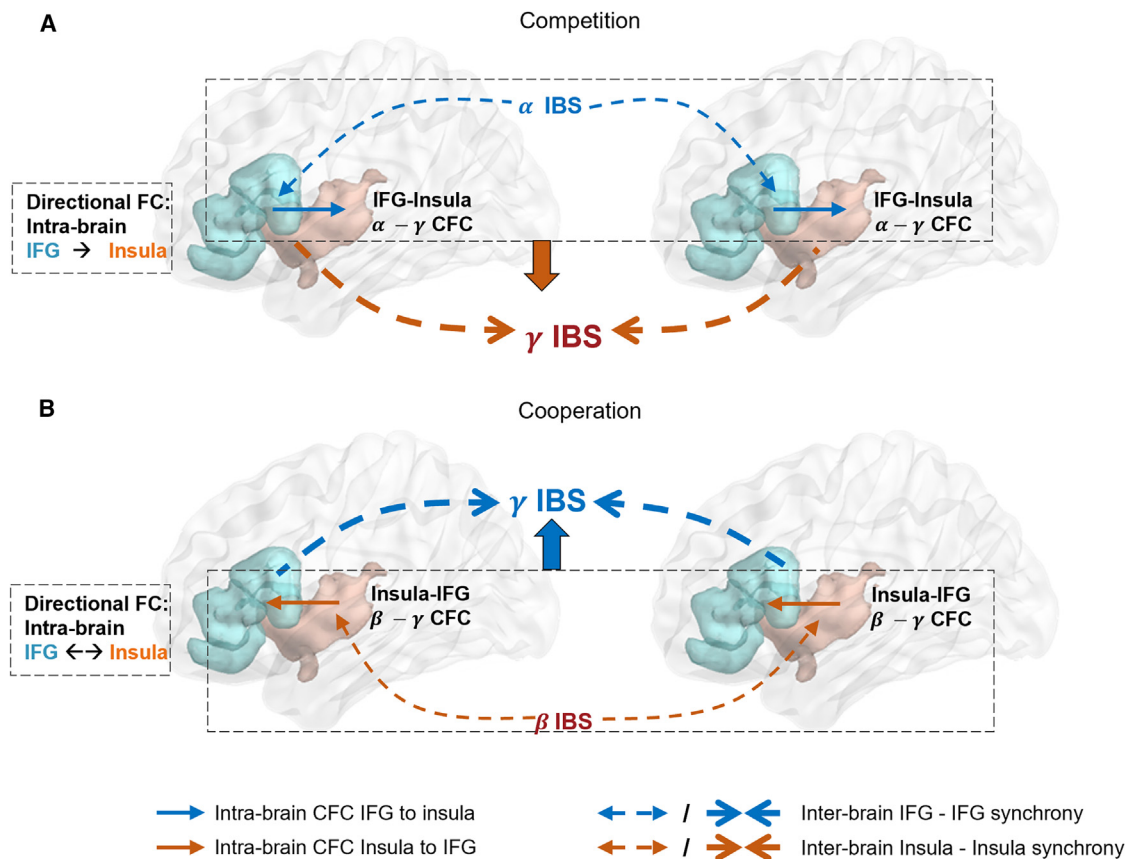


**Figure 5. The neural interaction and synchronization patterns of intra- and inter-brain insula-IFG during competition and cooperation tasks**

(A) During the competition, the IFG is illustrated as the predominant influence within the intra-brain insula-IFG circuitry, depicted by the dashed box on the left side of the figure (FC: Functional connectivity). The gamma band IBS of the insula can be explained by the alpha band IBS of the IFG and the intra-brain alpha-gamma coupling from IFG to insula (CFC: Cross-frequency coupling).

(B) During the cooperation, there is a balanced bidirectional interaction between the insula and IFG, as depicted in the dashed box on the left side of the figure. The gamma band IBS of the IFG can be explained by the beta band IBS of the insula and the intra-brain beta-gamma coupling from the insula to the IFG. (IFG in aqua; Insula in orange; Intra-brain CFC from IFG to insula: Solid blue arrows; Intra-brain CFC from insula to IFG: Solid orange arrows; Inter-brain IFG-IFG synchrony: Dashed blue arrows. Inter-brain insula-insula synchrony: Dashed orange arrows. Thicker dashed arrows pointing toward the center represent the explained gamma IBS, while thinner dashed arrows pointing to the sides represent the IBS used to support the gamma IBS explanation).

was small. While we used multiple analysis methods and obtained relatively consistent results to ensure robustness, these findings should be considered preliminary. Further studies with larger, more diverse samples are needed to extend our findings. Third, the controlled nature of our experimental paradigm, while useful for isolating specific neural mechanisms, does not fully capture the complexity of real-world social interactions. Our simplified model of cooperation and competition may not reflect the richness of social behaviors outside the laboratory setting. Future research should adopt more naturalistic paradigms, such as face-to-face interactions, to enhance ecological validity and provide more generalizable insights into the neural mechanisms of social behavior. Additionally, while our study focused on the insula and IFG due to their established roles in social cognition, we recognize that other brain regions—such as the right temporoparietal junction (rTPJ), right posterior superior temporal sulcus (pSTS), right inferior parietal lobule (IPL), and the cingulate cortex—are also critical components of the social

cognition network. These regions interact with the insula and IFG to support complex social interactions. Future research should incorporate these additional regions and explore their dynamic interplay in more ecologically valid social contexts, providing a more comprehensive understanding of the neural mechanisms underlying social interactions.

#### RESOURCE AVAILABILITY

##### Lead contact

Further information and requests for resources should be directed to and will be fulfilled by the lead contact, Junsong Zhang ([zhangjs@xmu.edu.cn](mailto:zhangjs@xmu.edu.cn)).

##### Materials availability

This study did not generate new unique reagents.

##### Data and code availability

- All data reported in this article will be shared by the lead contact upon request.

- This paper does not report the original code.
- Any additional information needed to reanalyze the data reported in this paper is available from the [lead contact](#) upon request.

## ACKNOWLEDGMENTS

This research was supported by the National Natural Science Foundation of China (No. 61772440, 62007016), the Collaborative Innovation Platform Project for Fuzhou-Xiamen-Quanzhou National Independent Innovation Demonstration Zone (No. 2022-P-028), the Project of Industry-university-research Collaborative Innovation in Fujian Province Universities (No. 2022Y4004), and the Xiamen Medical Health Science and Technology Project (No. 3502Z20194098).

## AUTHOR CONTRIBUTIONS

Conceptualization, X.Q., R.L., and J.Z.; methodology, X.Q., R.L., H.H., and Y.H.; investigation, X.Q., H.H., X.L., Z.L., S.C., L.Y., and S.T.O.; formal analysis, X.Q., S.T.O., and Y.H.; writing – original draft, X.Q.; writing – review and editing, X.Q., R.L., and J.Z.; visualization, X.Q. and R.L.; resources, Y.Y., F.W., X.Z., K.M.L., Y.X., and M.W.; funding acquisition, J.Z., R.L., and F.W.; supervision, J.Z.

## DECLARATION OF INTERESTS

The authors declare no competing interests.

## STAR★METHODS

Detailed methods are provided in the online version of this paper and include the following:

- **KEY RESOURCES TABLE**
- **EXPERIMENTAL MODEL AND STUDY PARTICIPANT DETAILS**
  - Participants
  - Experimental procedure
- **METHOD DETAILS**
  - Stereo-EEG data acquisition
  - Electrode localization
  - Behavioral analysis
  - SEEG preprocessing
  - Frequency band segmentation and implications
  - Time-frequency analysis
  - High-gamma frequency activity
  - Electrode selection
  - Intra-brain phase synchrony
  - Envelope-to-signal coupling
  - Phase slope index
  - Granger causality
  - Inter-brain coherence
- **QUANTIFICATION AND STATISTICAL ANALYSIS**

## SUPPLEMENTAL INFORMATION

Supplemental information can be found online at <https://doi.org/10.1016/j.isci.2024.111506>.

Received: July 20, 2024

Revised: September 2, 2024

Accepted: November 27, 2024

Published: November 29, 2024

## REFERENCES

1. Declerck, C.H., and Boone, C. (2018). The neuroeconomics of cooperation. *Nat. Human Behav.* 2, 438–440. <https://doi.org/10.1038/s41562-018-0387-3>.
2. Decety, J., Jackson, P.L., Sommerville, J.A., Chaminade, T., and Meltzoff, A.N. (2004). The neural bases of cooperation and competition: an fMRI investigation. *Neuroimage* 23, 744–751. <https://doi.org/10.1016/j.neuroimage.2004.05.025>.
3. Beauchamp, M.H., and Anderson, V. (2010). SOCIAL: An integrative framework for the development of social skills. *Psychol. Bull.* 136, 39–64. <https://doi.org/10.1037/a0017768>.
4. Hari, R., and Kujala, M.V. (2009). Brain Basis of Human Social Interaction: From Concepts to Brain Imaging. *Physiol. Rev.* 89, 453–479. <https://doi.org/10.1152/physrev.00041.2007>.
5. Balconi, M., and Vanutelli, M.E. (2017). Cooperation and Competition with Hyperscanning Methods: Review and Future Application to Emotion Domain. *Front. Comput. Neurosci.* 11, 86. <https://doi.org/10.3389/fncom.2017.00086>.
6. Cristofori, I., Cohen-Zimmerman, S., and Grafman, J. (2019). Chapter 11 - Executive functions. In *Handbook of Clinical Neurology The Frontal Lobes*, M. D'Esposito and J.H. Grafman, eds. (Elsevier), pp. 197–219. <https://doi.org/10.1016/B978-0-12-804281-6.00011-2>.
7. Gilbert, S.J., and Burgess, P.W. (2008). Executive function. *Curr. Biol.* 18, R110–R114. <https://doi.org/10.1016/j.cub.2007.12.014>.
8. Frith, C.D., and Frith, U. (2006). The Neural Basis of Mentalizing. *Neuron* 50, 531–534. <https://doi.org/10.1016/j.neuron.2006.05.001>.
9. Frith, C.D., and Frith, U. (2012). Mechanisms of Social Cognition. *Annu. Rev. Psychol.* 63, 287–313. <https://doi.org/10.1146/annurev-psych-120710-100449>.
10. Lotter, L.D., Kohl, S.H., Gerloff, C., Bell, L., Niephaus, A., Kruppa, J.A., Dukat, J., Schulte-Rüther, M., Reindl, V., and Konrad, K. (2023). Revealing the neurobiology underlying interpersonal neural synchronization with multimodal data fusion. *Neurosci. Biobehav. Rev.* 146, 105042. <https://doi.org/10.1016/j.neubiorev.2023.105042>.
11. Redcay, E., and Schilbach, L. (2019). Using second-person neuroscience to elucidate the mechanisms of social interaction. *Nat. Rev. Neurosci.* 20, 495–505. <https://doi.org/10.1038/s41583-019-0179-4>.
12. Aron, A.R., Fletcher, P.C., Bullmore, E.T., Sahakian, B.J., and Robbins, T.W. (2003). Stop-signal inhibition disrupted by damage to right inferior frontal gyrus in humans. *Nat. Neurosci.* 6, 115–116. <https://doi.org/10.1038/nn1003>.
13. Swick, D., Ashley, V., and Turken, A.U. (2008). Left inferior frontal gyrus is critical for response inhibition. *BMC Neurosci.* 9, 102. <https://doi.org/10.1186/1471-2202-9-102>.
14. Iacoboni, M., and Dapretto, M. (2006). The mirror neuron system and the consequences of its dysfunction. *Nat. Rev. Neurosci.* 7, 942–951. <https://doi.org/10.1038/nrn2024>.
15. Catmur, C. (2015). Understanding intentions from actions: Direct perception, inference, and the roles of mirror and mentalizing systems. *Conscious. Cognit.* 36, 426–433. <https://doi.org/10.1016/j.concog.2015.03.012>.
16. Van Overwalle, F., and Baetens, K. (2009). Understanding others' actions and goals by mirror and mentalizing systems: A meta-analysis. *Neuroimage* 48, 564–584. <https://doi.org/10.1016/j.neuroimage.2009.06.009>.
17. Decety, J. (2011). Dissecting the Neural Mechanisms Mediating Empathy. *Emot. Rev.* 3, 92–108. <https://doi.org/10.1177/1754073910374662>.
18. Shamay-Tsoory, S.G., Aharon-Peretz, J., and Perry, D. (2009). Two systems for empathy: a double dissociation between emotional and cognitive empathy in inferior frontal gyrus versus ventromedial prefrontal lesions. *Brain* 132, 617–627. <https://doi.org/10.1093/brain/awn279>.
19. Liu, T., Saito, H., and Oi, M. (2015). Role of the right inferior frontal gyrus in turn-based cooperation and competition: A near-infrared spectroscopy study. *Brain Cognit.* 99, 17–23. <https://doi.org/10.1016/j.bandc.2015.07.001>.
20. Liu, T., Saito, G., Lin, C., and Saito, H. (2017). Inter-brain network underlying turn-based cooperation and competition: A hyperscanning study using

- near-infrared spectroscopy. *Sci. Rep.* 7, 8684. <https://doi.org/10.1038/s41598-017-09226-w>.
21. Osaka, N., Minamoto, T., Yaoi, K., Azuma, M., Shimada, Y.M., and Osaka, M. (2015). How Two Brains Make One Synchronized Mind in the Inferior Frontal Cortex: fNIRS-Based Hyperscanning During Cooperative Singing. *Front. Psychol.* 6, 1811.
  22. Schurz, M., and Tholen, M.G. (2016). What brain imaging did (not) tell us about the Inferior Frontal Gyrus in theory of mind – A commentary on Samson et al., (2015). *Cortex* 74, 329–333. <https://doi.org/10.1016/j.cortex.2015.08.011>.
  23. Corbetta, M., Patel, G., and Shulman, G.L. (2008). The Reorienting System of the Human Brain: From Environment to Theory of Mind. *Neuron* 58, 306–324. <https://doi.org/10.1016/j.neuron.2008.04.017>.
  24. Frith, C.D., and Frith, U. (1999). Interacting Minds—A Biological Basis. *Science* 286, 1692–1695. <https://doi.org/10.1126/science.286.5445.1692>.
  25. Huang, Z., Tarnal, V., Vlisides, P.E., Janke, E.L., McKinney, A.M., Picton, P., Mashour, G.A., and Hudetz, A.G. (2021). Anterior insula regulates brain network transitions that gate conscious access. *Cell Rep.* 35, 109081. <https://doi.org/10.1016/j.celrep.2021.109081>.
  26. Shamay-Tsoory, S.G., Saporta, N., Marton-Alper, I.Z., and Gvirts, H.Z. (2019). Herding Brains: A Core Neural Mechanism for Social Alignment. *Trends Cognit. Sci.* 23, 174–186. <https://doi.org/10.1016/j.tics.2019.01.002>.
  27. Molnar-Szakacs, I., and Uddin, L.Q. (2022). Anterior insula as a gatekeeper of executive control. *Neurosci. Biobehav. Rev.* 139, 104736. <https://doi.org/10.1016/j.neubiorev.2022.104736>.
  28. Sridharan, D., Levitin, D.J., and Menon, V. (2008). A critical role for the right fronto-insular cortex in switching between central-executive and default-mode networks. *Proc. Natl. Acad. Sci. USA* 105, 12569–12574. <https://doi.org/10.1073/pnas.0800005105>.
  29. Dionisio, S., Mayoglou, L., Cho, S.-M., Prime, D., Flanigan, P.M., Lega, B., Mosher, J., Leahy, R., Gonzalez-Martinez, J., and Nair, D. (2019). Connectivity of the human insula: A cortico-cortical evoked potential (CCEP) study. *Cortex* 120, 419–442. <https://doi.org/10.1016/j.cortex.2019.05.019>.
  30. Rilling, J.K., Goldsmith, D.R., Glenn, A.L., Jairam, M.R., Elfenbein, H.A., Dagenais, J.E., Murdock, C.D., and Pagnoni, G. (2008). The neural correlates of the affective response to unreciprocated cooperation. *Neuropsychologia* 46, 1256–1266. <https://doi.org/10.1016/j.neuropsychologia.2007.11.033>.
  31. Montague, P.R., Berns, G.S., Cohen, J.D., McClure, S.M., Pagnoni, G., Dhamala, M., Wiest, M.C., Karpov, I., King, R.D., Apple, N., and Fisher, R.E. (2002). Hyperscanning: Simultaneous fMRI during Linked Social Interactions. *Neuroimage* 16, 1159–1164. <https://doi.org/10.1006/nimg.2002.1150>.
  32. Babiloni, F., and Astolfi, L. (2014). Social neuroscience and hyperscanning techniques: Past, present and future. *Neurosci. Biobehav. Rev.* 44, 76–93. <https://doi.org/10.1016/j.neubiorev.2012.07.006>.
  33. Hamilton, A.F.D.C. (2021). Hyperscanning: Beyond the Hype. *Neuron* 109, 404–407. <https://doi.org/10.1016/j.neuron.2020.11.008>.
  34. Friston, K.J., and Frith, C.D. (2015). Active inference, communication and hermeneutics. *Cortex* 68, 129–143. <https://doi.org/10.1016/j.cortex.2015.03.025>.
  35. Cui, X., Bryant, D.M., and Reiss, A.L. (2012). NIRS-based hyperscanning reveals increased interpersonal coherence in superior frontal cortex during cooperation. *Neuroimage* 59, 2430–2437. <https://doi.org/10.1016/j.neuroimage.2011.09.003>.
  36. Szymanski, C., Pesquita, A., Brennan, A.A., Perdakis, D., Enns, J.T., Brick, T.R., Müller, V., and Lindenberger, U. (2017). Teams on the same wavelength perform better: Inter-brain phase synchronization constitutes a neural substrate for social facilitation. *Neuroimage* 152, 425–436. <https://doi.org/10.1016/j.neuroimage.2017.03.013>.
  37. Marton-Alper, I.Z., Markus, A., Nevat, M., Bennet, R., and Shamay-Tsoory, S.G. (2023). Differential contribution of between and within-brain coupling to movement synchronization. *Hum. Brain Mapp.* 44, 4136–4151. <https://doi.org/10.1002/hbm.26335>.
  38. Koike, T., Tanabe, H.C., Okazaki, S., Nakagawa, E., Sasaki, A.T., Shimada, K., Sugawara, S.K., Takahashi, H.K., Yoshihara, K., Bosch-Bayard, J., and Sadato, N. (2016). Neural substrates of shared attention as social memory: A hyperscanning functional magnetic resonance imaging study. *Neuroimage* 125, 401–412. <https://doi.org/10.1016/j.neuroimage.2015.09.076>.
  39. Shaw, D.J., Czekóová, K., Staněk, R., Mareček, R., Urbánek, T., Špalek, J., Kopečková, L., Řezáč, J., and Brázdil, M. (2018). A dual-fMRI investigation of the iterated Ultimatum Game reveals that reciprocal behaviour is associated with neural alignment. *Sci. Rep.* 8, 10896. <https://doi.org/10.1038/s41598-018-29233-9>.
  40. Xie, H., Karipidis, I.I., Howell, A., Schreier, M., Sheau, K.E., Manchanda, M.K., Ayub, R., Glover, G.H., Jung, M., Reiss, A.L., and Saggat, M. (2020). Finding the neural correlates of collaboration using a three-person fMRI hyperscanning paradigm. *Proc. Natl. Acad. Sci. USA* 117, 23066–23072. <https://doi.org/10.1073/pnas.1917407117>.
  41. Yoshioka, A., Tanabe, H.C., Sumiya, M., Nakagawa, E., Okazaki, S., Koike, T., and Sadato, N. (2021). Neural substrates of shared visual experiences: a hyperscanning fMRI study. *Soc. Cognit. Affect Neurosci.* 16, 1264–1275. <https://doi.org/10.1093/scan/nsab082>.
  42. Wood, J.N., and Grafman, J. (2003). Human prefrontal cortex: processing and representational perspectives. *Nat. Rev. Neurosci.* 4, 139–147. <https://doi.org/10.1038/nrn1033>.
  43. Bonnefond, M., Kastner, S., and Jensen, O. (2017). Communication between Brain Areas Based on Nested Oscillations. *eNeuro* 4, ENEURO.0153-16.2017. <https://doi.org/10.1523/ENEURO.0153-16.2017>.
  44. Fries, P. (2005). A mechanism for cognitive dynamics: neuronal communication through neuronal coherence. *Trends Cognit. Sci.* 9, 474–480. <https://doi.org/10.1016/j.tics.2005.08.011>.
  45. Varela, F., Lachaux, J.-P., Rodriguez, E., and Martinerie, J. (2001). The brainweb: Phase synchronization and large-scale integration. *Nat. Rev. Neurosci.* 2, 229–239. <https://doi.org/10.1038/35067550>.
  46. Logothetis, N.K. (2008). What we can do and what we cannot do with fMRI. *Nature* 453, 869–878. <https://doi.org/10.1038/nature06976>.
  47. Riggs, L., Moses, S.N., Bardouille, T., Herdman, A.T., Ross, B., and Ryan, J.D. (2009). A complementary analytic approach to examining medial temporal lobe sources using magnetoencephalography. *Neuroimage* 45, 627–642. <https://doi.org/10.1016/j.neuroimage.2008.11.018>.
  48. Liu, J., and Xue, G. (2023). What Is the Contribution of iEEG as Compared to Other Methods to Cognitive Neuroscience? In *Intracranial EEG: A Guide for Cognitive Neuroscientists Studies in Neuroscience*. In Psychology and Behavioral Economics, N. Axmacher, ed. (Springer International Publishing), pp. 103–124. [https://doi.org/10.1007/978-3-031-20910-9\\_8](https://doi.org/10.1007/978-3-031-20910-9_8).
  49. Leszczyński, M., Barczak, A., Kajikawa, Y., Ulbert, I., Falchier, A.Y., Tal, I., Haegens, S., Melloni, L., Knight, R.T., and Schroeder, C.E. (2020). Dissociation of broadband high-frequency activity and neuronal firing in the neocortex. *Sci. Adv.* 6, eabb0977. <https://doi.org/10.1126/sciadv.abb0977>.
  50. Nir, Y., Fisch, L., Mukamel, R., Gelbard-Sagiv, H., Arieli, A., Fried, I., and Malach, R. (2007). Coupling between Neuronal Firing Rate, Gamma LFP, and BOLD fMRI Is Related to Interneuronal Correlations. *Curr. Biol.* 17, 1275–1285. <https://doi.org/10.1016/j.cub.2007.06.066>.
  51. Rich, E.L., and Wallis, J.D. (2017). Spatiotemporal dynamics of information encoding revealed in orbitofrontal high-gamma. *Nat. Commun.* 8, 1139. <https://doi.org/10.1038/s41467-017-01253-5>.
  52. Mukamel, R., Gelbard, H., Arieli, A., Hasson, U., Fried, I., and Malach, R. (2005). Coupling Between Neuronal Firing, Field Potentials, and fMRI in Human Auditory Cortex. *Science* 309, 951–954. <https://doi.org/10.1126/science.1110913>.

53. Niessing, J., Ebisch, B., Schmidt, K.E., Niessing, M., Singer, W., and Galuske, R.A.W. (2005). Hemodynamic Signals Correlate Tightly with Synchronized Gamma Oscillations. *Science* 309, 948–951. <https://doi.org/10.1126/science.1110948>.
54. Vinck, M., Oostenveld, R., van Wingerden, M., Battaglia, F., and Pennartz, C.M.A. (2011). An improved index of phase-synchronization for electrophysiological data in the presence of volume-conduction, noise and sample-size bias. *Neuroimage* 55, 1548–1565. <https://doi.org/10.1016/j.neuroimage.2011.01.055>.
55. Balconi, M., and Angioletti, L. (2022). Neuroscience and Competitive Behavior. In *The Oxford Handbook of the Psychology of Competition*, S.M. Garcia, A. Tor, and A.J. Elliot, eds. (Oxford University Press), pp. 117–133. <https://doi.org/10.1093/oxfordhb/9780190060800.013.27>.
56. Bruns, A., and Eckhorn, R. (2004). Task-related coupling from high- to low-frequency signals among visual cortical areas in human subdural recordings. *Int. J. Psychophysiol.* 51, 97–116. <https://doi.org/10.1016/j.ijpsycho.2003.07.001>.
57. Nolte, G., Ziehe, A., Nikulin, V.V., Schlögl, A., Krämer, N., Brismar, T., and Müller, K.-R. (2008). Robustly Estimating the Flow Direction of Information in Complex Physical Systems. *Phys. Rev. Lett.* 100, 234101. <https://doi.org/10.1103/PhysRevLett.100.234101>.
58. Balconi, M., and Fronda, G. (2021). Intra-Brain Connectivity vs. Inter-Brain Connectivity in Gestures Reproduction: What Relationship? *Brain Sci.* 11, 577. <https://doi.org/10.3390/brainsci11050577>.
59. Vicente, U., Ara, A., and Marco-Pallarés, J. (2023). Intra- and inter-brain synchrony oscillations underlying social adjustment. *Sci. Rep.* 13, 11211. <https://doi.org/10.1038/s41598-023-38292-6>.
60. Fox, M.D., Corbetta, M., Snyder, A.Z., Vincent, J.L., and Raichle, M.E. (2006). Spontaneous neuronal activity distinguishes human dorsal and ventral attention systems. *Proc. Natl. Acad. Sci. USA* 103, 10046–10051. <https://doi.org/10.1073/pnas.0604187103>.
61. Greicius, M.D., Krasnow, B., Reiss, A.L., and Menon, V. (2003). Functional connectivity in the resting brain: A network analysis of the default mode hypothesis. *Proc. Natl. Acad. Sci. USA* 100, 253–258. <https://doi.org/10.1073/pnas.0135058100>.
62. Menon, V., and Uddin, L.Q. (2010). Saliency, switching, attention and control: a network model of insula function. *Brain Struct. Funct.* 214, 655–667. <https://doi.org/10.1007/s00429-010-0262-0>.
63. Braga, R.M., Wilson, L.R., Sharp, D.J., Wise, R.J.S., and Leech, R. (2013). Separable networks for top-down attention to auditory non-spatial and visuospatial modalities. *Neuroimage* 74, 77–86. <https://doi.org/10.1016/j.neuroimage.2013.02.023>.
64. Kilner, J.M., Neal, A., Weiskopf, N., Friston, K.J., and Frith, C.D. (2009). Evidence of Mirror Neurons in Human Inferior Frontal Gyrus. *J. Neurosci.* 29, 10153–10159. <https://doi.org/10.1523/JNEUROSCI.2668-09.2009>.
65. Buccino, G., Vogt, S., Ritzl, A., Fink, G.R., Zilles, K., Freund, H.-J., and Rizzolatti, G. (2004). Neural Circuits Underlying Imitation Learning of Hand Actions: An Event-Related fMRI Study. *Neuron* 42, 323–334. [https://doi.org/10.1016/S0896-6273\(04\)00181-3](https://doi.org/10.1016/S0896-6273(04)00181-3).
66. Barraza, P., Pérez, A., and Rodríguez, E. (2020). Brain-to-Brain Coupling in the Gamma-Band as a Marker of Shared Intentionality. *Front. Hum. Neurosci.* 14, 295. <https://doi.org/10.3389/fnhum.2020.00295>.
67. Buzsáki, G. (2006). *Rhythms of the Brain* (Oxford University Press).
68. Clayton, M.S., Yeung, N., and Cohen Kadosh, R. (2015). The roles of cortical oscillations in sustained attention. *Trends Cognit. Sci.* 19, 188–195. <https://doi.org/10.1016/j.tics.2015.02.004>.
69. Hur, J., Miller, G.A., McDevitt, J.R.B., Spielberg, J.M., Crocker, L.D., Infantolino, Z.P., Towers, D.N., Warren, S.L., and Heller, W. (2015). Interactive effects of trait and state affect on top-down control of attention. *Soc. Cognit. Affect Neurosci.* 10, 1128–1136. <https://doi.org/10.1093/scan/nsu163>.
70. Betti, V., Zappasodi, F., Rossini, P.M., Aglioti, S.M., and Tecchio, F. (2009). Synchronous with Your Feelings: Sensorimotor  $\gamma$  Band and Empathy for Pain. *J. Neurosci.* 29, 12384–12392. <https://doi.org/10.1523/JNEUROSCI.2759-09.2009>.
71. Djalovski, A., Dumas, G., Kinreich, S., and Feldman, R. (2021). Human attachments shape interbrain synchrony toward efficient performance of social goals. *Neuroimage* 226, 117600. <https://doi.org/10.1016/j.neuroimage.2020.117600>.
72. Mu, Y., Han, S., and Gelfand, M.J. (2017). The role of gamma interbrain synchrony in social coordination when humans face territorial threats. *Soc. Cogn. Affect. Neuroscience* 12, 1614–1623. <https://doi.org/10.1093/scan/nsx093>.
73. Cohen, M.X., David, N., Vogeley, K., and Elger, C.E. (2009). Gamma-band activity in the human superior temporal sulcus during mentalizing from nonverbal social cues. *Psychophysiology* 46, 43–51. <https://doi.org/10.1111/j.1469-8986.2008.00724.x>.
74. Moreau, Q., Adel, L., Douglas, C., Ranjbaran, G., and Dumas, G. (2022). A neurodynamic model of inter-brain coupling in the gamma band. *J. Neurophysiol.* 128, 1085–1090. <https://doi.org/10.1152/jn.00224.2022>.
75. Cheng, X., Li, X., and Hu, Y. (2015). Synchronous brain activity during cooperative exchange depends on gender of partner: A fNIRS-based hyperscanning study. *Hum. Brain Mapp.* 36, 2039–2048. <https://doi.org/10.1002/hbm.22754>.
76. Pan, Y., Cheng, X., Zhang, Z., Li, X., and Hu, Y. (2017). Cooperation in lovers: An fNIRS-based hyperscanning study: Cooperation in Lovers. *Hum. Brain Mapp.* 38, 831–841. <https://doi.org/10.1002/hbm.23421>.
77. Zheng, J., Stevenson, R.F., Mander, B.A., Mnatsakanyan, L., Hsu, F.P.K., Vadera, S., Knight, R.T., Yassa, M.A., and Lin, J.J. (2019). Multiplexing of Theta and Alpha Rhythms in the Amygdala-Hippocampal Circuit Supports Pattern Separation of Emotional Information. *Neuron* 102, 887–898.e5. <https://doi.org/10.1016/j.neuron.2019.03.025>.
78. Parvizi, J., and Kastner, S. (2018). Promises and limitations of human intracranial electroencephalography. *Nat. Neurosci.* 21, 474–483. <https://doi.org/10.1038/s41593-018-0108-2>.
79. Nasreddine, Z.S., Phillips, N.A., Bédirian, V., Charbonneau, S., Whitehead, V., Collin, I., Cummings, J.L., and Chertkow, H. (2005). The Montreal Cognitive Assessment, MoCA: A Brief Screening Tool For Mild Cognitive Impairment. *J. Am. Geriatr. Soc.* 53, 695–699. <https://doi.org/10.1111/j.1532-5415.2005.53221.x>.
80. Delorme, A., and Makeig, S. (2004). EEGLAB: an open source toolbox for analysis of single-trial EEG dynamics including independent component analysis. *J. Neurosci. Methods* 134, 9–21. <https://doi.org/10.1016/j.jneumeth.2003.10.009>.
81. Oostenveld, R., Fries, P., Maris, E., and Schoffelen, J.-M. (2011). FieldTrip: open source software for advanced analysis of MEG, EEG, and invasive electrophysiological data. *Comput. Intell. Neurosci.* 2011, 156869. <https://doi.org/10.1155/2011/156869>.
82. Fischl, B. (2012). FreeSurfer. *Neuroimage* 62, 774–781. <https://doi.org/10.1016/j.neuroimage.2012.01.021>.
83. Groppe, D.M., Bickel, S., Dykstra, A.R., Wang, X., Mégevand, P., Mercier, M.R., Lado, F.A., Mehta, A.D., and Honey, C.J. (2017). iELVis: An open source MATLAB toolbox for localizing and visualizing human intracranial electrode data. *J. Neurosci. Methods* 281, 40–48. <https://doi.org/10.1016/j.jneumeth.2017.01.022>.
84. Fischl, B., Sereno, M.I., Tootell, R.B., and Dale, A.M. (1999). High-resolution intersubject averaging and a coordinate system for the cortical surface. *Hum. Brain Mapp.* 8, 272–284. [https://doi.org/10.1002/\(SICI\)1097-0193\(1999\)8:4<272::AID-HBM10>3.0.CO](https://doi.org/10.1002/(SICI)1097-0193(1999)8:4<272::AID-HBM10>3.0.CO).
85. Xia, M., Wang, J., and He, Y. (2013). BrainNet Viewer: A Network Visualization Tool for Human Brain Connectomics. *PLoS One* 8, e68910. <https://doi.org/10.1371/journal.pone.0068910>.
86. Li, G., Jiang, S., Paraskevopoulou, S.E., Wang, M., Xu, Y., Wu, Z., Chen, L., Zhang, D., and Schalk, G. (2018). Optimal referencing for stereo-electroencephalographic (SEEG) recordings. *Neuroimage* 183, 327–335. <https://doi.org/10.1016/j.neuroimage.2018.08.020>.

87. Han, C., Wang, T., Yang, Y., Wu, Y., Li, Y., Dai, W., Zhang, Y., Wang, B., Yang, G., Cao, Z., et al. (2021). Multiple gamma rhythms carry distinct spatial frequency information in primary visual cortex. *PLoS Biol.* *19*, e3001466. <https://doi.org/10.1371/journal.pbio.3001466>.
88. Sonkusare, S., Nguyen, V.T., Moran, R., Van Der Meer, J., Ren, Y., Kousis, N., Dionisio, S., Breakspear, M., and Guo, C. (2020). Intracranial-EEG evidence for medial temporal pole driving amygdala activity induced by multi-modal emotional stimuli. *Cortex* *130*, 32–48. <https://doi.org/10.1016/j.cortex.2020.05.018>.
89. Kosciessa, J.Q., Grandy, T.H., Garrett, D.D., and Werkle-Bergner, M. (2020). Single-trial characterization of neural rhythms: Potential and challenges. *Neuroimage* *206*, 116331. <https://doi.org/10.1016/j.neuroimage.2019.116331>.
90. Li, J., Cao, D., Yu, S., Xiao, X., Imbach, L., Stieglitz, L., Sarnthein, J., and Jiang, T. (2023). Functional specialization and interaction in the amygdala-hippocampus circuit during working memory processing. *Nat. Commun.* *14*, 2921. <https://doi.org/10.1038/s41467-023-38571-w>.
91. Foster, B.L., Rangarajan, V., Shirer, W.R., and Parvizi, J. (2015). Intrinsic and Task-Dependent Coupling of Neuronal Population Activity in Human Parietal Cortex. *Neuron* *86*, 578–590. <https://doi.org/10.1016/j.neuron.2015.03.018>.
92. Oehm, C.R., Hanslmayr, S., Fell, J., Deuker, L., Kremers, N.A., Do Lam, A.T., Elger, C.E., and Axmacher, N. (2014). Neural Communication Patterns Underlying Conflict Detection, Resolution, and Adaptation. *J. Neurosci.* *34*, 10438–10452. <https://doi.org/10.1523/JNEUROSCI.3099-13.2014>.
93. Maris, E., and Oostenveld, R. (2007). Nonparametric statistical testing of EEG- and MEG-data. *J. Neurosci. Methods* *164*, 177–190. <https://doi.org/10.1016/j.jneumeth.2007.03.024>.
94. Onslow, A.C.E., Bogacz, R., and Jones, M.W. (2011). Quantifying phase-amplitude coupling in neuronal network oscillations. *Prog. Biophys. Mol. Biol.* *105*, 49–57. <https://doi.org/10.1016/j.pbiomolbio.2010.09.007>.
95. Johnson, E.L., Adams, J.N., Solbakk, A.-K., Endestad, T., Larsson, P.G., Ivanovic, J., Meling, T.R., Lin, J.J., and Knight, R.T. (2018). Dynamic frontotemporal systems process space and time in working memory. *PLoS Biol.* *16*, e2004274. <https://doi.org/10.1371/journal.pbio.2004274>.
96. Bressler, S.L., and Seth, A.K. (2011). Wiener–Granger Causality: A well established methodology. *Neuroimage* *58*, 323–329. <https://doi.org/10.1016/j.neuroimage.2010.02.059>.
97. Granger, C.W.J. (1969). Investigating Causal Relations by Econometric Models and Cross-spectral Methods. *Econometrica* *37*, 424–438. <https://doi.org/10.2307/1912791>.
98. Barnett, L., and Seth, A.K. (2014). The MVGC multivariate Granger causality toolbox: A new approach to Granger-causal inference. *J. Neurosci. Methods* *223*, 50–68. <https://doi.org/10.1016/j.jneumeth.2013.10.018>.

## STAR★METHODS

## KEY RESOURCES TABLE

REAGENT or RESOURCE	SOURCE	IDENTIFIER
Software and algorithms		
MATLAB 2021a	<a href="https://ww2.mathworks.cn/products/matlab.html">https://ww2.mathworks.cn/products/matlab.html</a>	RRID: SCR_001622
FreeSurfer	<a href="https://surfer.nmr.mgh.harvard.edu/">https://surfer.nmr.mgh.harvard.edu/</a>	RRID: SCR_001847
BioImage Suite 30_1_03_17_2011	<a href="https://bioimagesuiteweb.github.io/webapp/index.html">https://bioimagesuiteweb.github.io/webapp/index.html</a>	RRID: SCR_002986
iELVis	<a href="http://ielvis.pbworks.com/w/page/116347253/FrontPage">http://ielvis.pbworks.com/w/page/116347253/FrontPage</a>	RRID: SCR_016109
EEGLAB 2021.0	<a href="https://sccn.ucsd.edu/eeglab/index.php">https://sccn.ucsd.edu/eeglab/index.php</a>	RRID: SCR_007292
FieldTrip 20221022	<a href="https://www.fieldtriptoolbox.org/">https://www.fieldtriptoolbox.org/</a>	RRID: SCR_004849
IBM SPSS V22.0	<a href="https://www.ibm.com/products/spss-statistics">https://www.ibm.com/products/spss-statistics</a>	RRID: SCR_016479
Multivariate Granger Causality (MVG C)	<a href="https://users.sussex.ac.uk/~lionelb/MVGC/">https://users.sussex.ac.uk/~lionelb/MVGC/</a>	RRID: SCR_015755

## EXPERIMENTAL MODEL AND STUDY PARTICIPANT DETAILS

## Participants

We recruited 16 patients (8 females, mean age:  $28.38 \pm 10.49$  years, 100% right-handed) at Xiamen Humanity Hospital (China) to form 8 pairs (see [Table S2](#) for detailed pairing information). All participants were diagnosed with drug-resistant epilepsy and underwent intracranial deep brain electrode implantation to localize the epileptic focus for treatment. The electrode placement was determined entirely based on clinical requirements. The Montreal Cognitive Assessment (MoCA)<sup>79</sup> was used to assess executive function in patients. To ensure the robustness of our study, we implemented a rigorous participant selection and matching procedure. A team of experienced clinical neurologists performed a comprehensive assessment of the participants' clinical characteristics, including seizure severity, electrode coverage, and cognitive function. Participants were then carefully matched to these variables to minimize the impact of individual differences. One patient (PT007) was excluded from the study due to the overlap of insula electrodes with the epileptogenic zone. Ultimately, the analysis encompassed a total of 15 patients for individual-level analysis, while 7 pairs for group-level analysis. Patient characteristics are provided in [Tables 1](#) and [S1](#). Before testing, all participants signed a written informed consent in accordance with the Xiamen Humanity Hospital, China.

## Experimental procedure

The experimental tasks were inspired by a previous study<sup>35</sup> and each pair was involved in two separate computer-based tasks: cooperation and competition. The order in which participants performed the two tasks was randomized. Participants either completed the cooperation task followed by the competition task, or vice versa. Before the formal experiment, each pair of participants completed a practice session to ensure that they were familiar with the rules of the two tasks. Each task in the formal experiment consisted of Rest 1 (30s), Block 1, Rest 2 (30s), Block 2, and Rest 3 (30s) ([Figure 1C](#)). One block contained 20 trials; each trial began with a 2s blank, followed by a hollow gray circle that appeared on the screen. This gray circle is a preparation cue that has a duration ranging from 0.6s to 1.5s. After that, the gray circle filled with a green circle is presented as the target cue. Once the target is present, participants are expected to respond using the keyboard, and upon completion, a 4s feedback is displayed for the cooperation task, while a 1.5s feedback is displayed for the competition task ([Figure 1D](#)). Detailed descriptions of the requirements of each task are provided below.

In the cooperation task, participants were instructed to press their own keys as simultaneously as possible. The equation below illustrates the threshold for determining successful cooperation between dyad members.

$$T = \frac{1}{8}(RT_1 + RT_2)$$

Where  $T$  is the threshold,  $RT_1$  and  $RT_2$  are the response times of the two participants. For each dyad, if the difference between the response times was below the threshold, they both won one point for successful cooperation; otherwise, both lost one point, and they could adjust their response times based on the 4s feedback display. The feedback displayed whether they won or lost, their cumulative points in this task, and who is faster (green "+") or slower (white "-").

In the competition task, participants were instructed to press their button as soon as possible. They needed to be faster than each other on the task to win. In each trial, the faster player won one point, while the slower one lost a point. Like the cooperative task, a 1.5s feedback screen was presented following the completion of the two participants' responses. This screen displayed the outcome of the dyad's performance, including the identification of the winner and loser, as well as their respective cumulative points in this task.

## METHOD DETAILS

### Stereo-EEG data acquisition

Intracerebral electrodes with multiple contacts (Sinovation, China, 8–16 contacts, electrode diameter: 0.8 mm, intercontact spacing: 1.5 mm) were implanted using a stereotactic procedure. The placement of these electrodes was individually planned based on the estimated seizure onset zone, determined by the epilepsy clinician. Participants were carefully selected to ensure that they had similar electrode implantations and cognitive abilities. Participants were paired and seated side by side on their respective beds in the same room, as shown in Figure 1A. Each participant had their own monitor and keyboard (client) in front of them, both connected to the same computer server. The server controlled the presentation of stimuli on the clients, ensuring that both participants saw the same content. The server also collected behavioral data such as button press response times from both participants. During the task, the server simultaneously sent markers (solid orange arrows in Figure 1A) to the two SEEG data acquisition amplifiers (NEUVO-256H system), which served as timestamps for synchronizing the SEEG data. SEEG signals sampled at 10,000 Hz were transmitted from amplifiers to a central hospital server for storage. Participants were separated by a curtain during the task, and they were instructed not to communicate or see each other's actions. All experimental data were analyzed using MATLAB (R2021a, the MathWorks, Natick, MA, USA) with EEGLAB<sup>80</sup> and FieldTrip<sup>81</sup> toolboxes for coding and offline processing. Some of the behavioral statistical analyses were performed using IBM SPSS version 22.

### Electrode localization

The localization of electrodes in each subject was achieved by using co-registered pre-implantation structural T1-weighted MRI and post-implantation computed tomography (CT) scans. First, we performed brain mapping segmentation of the pre-implantation MRI using FreeSurfer.<sup>82</sup> Second, we registered post-implantation CT to the pre-implantation MRI. Then, we used Biolumage Suite (<https://bioimagesuite.org>) to localize electrodes in the co-registered CT. Finally, we used the freely available iELVis toolbox (<https://github.com/iELVis/iELVis>)<sup>83</sup> to expert electrode position information and map electrodes to the FreeSurfer average brain.<sup>84</sup> Based on the localization of the electrodes, we selected one electrode each from the ipsilateral insula and inferior frontal gyrus of each participant, both of which exhibited significant change during the task compared to the baseline (see Electrode selection for details). The electrode channels from the insula and IFG were mapped onto the Montreal Neurological Institute (MNI) space using the BrainNet Viewer<sup>85</sup> (Figure 1B). The corresponding MNI coordinates are detailed in Table S3.

### Behavioral analysis

We analyzed the response times (RTs) of participants in different tasks. To reduce the impact of outliers on subsequent data analysis, we calculated the mean and standard deviation (SD) of RTs for each participant in different tasks. Then, we excluded trials with RTs beyond the range of mean  $\pm 3$  SD.<sup>76</sup> At the same time, these trials were also excluded from subsequent SEEG data analysis. Specifically, 13.75% of competitive trials and 5% of cooperative trials were excluded due to RTs exceeding the threshold. For both tasks, we calculated the overall mean RT and the mean RT per block after removing outlier RTs from 15 participants. To measure the closeness of button response between pair members, we calculated the difference ( $\Delta$ RT) between the RTs of the two participants in the same group. As the data were not normally distributed, nonparametric Wilcoxon tests were conducted on the RTs and  $\Delta$ RTs between cooperation and competition tasks. To investigate the temporal evolution of behavioral and neural responses during cooperation, we calculated the overall percentage of winning trials (PWT) for each pair and the PWT for each block. Furthermore, we conducted Wilcoxon rank-sum tests to examine the trial-by-trial differences in response time between the two participants between the two blocks. Given the normal distribution of the data, a paired-sample t-test was used to examine the differences between the two blocks.

### SEEG preprocessing

The SEEG signals were down sampled at 2000 Hz and then referenced using the Laplacian method. The local Laplacian derivative has been proved to minimize cross-channel correlation, thereby maximizing the reduction of far-field volume conduction.<sup>86</sup> The Laplacian reference was computed by averaging the signals from neighboring channels and subtracting this average from the signal at the channel of interest.<sup>86</sup> The referenced signal is described by the following formula:

$$S'_i = S_i - \frac{1}{2}(S_{i-1} + S_{i+1})$$

For channels located at the top and bottom of the electrode shaft, we simplified the equation to  $S'_i = S_i - S_{i-1}$  and  $S'_i = S_i - S_{i+1}$ , respectively, as described by Li et al.<sup>86</sup> Prior to subsequent data processing, all channels identified as being within the epileptogenic zone or electrodes with excessive line noise<sup>86</sup> were excluded from the data analysis. The line noise of each channel ( $X_{LN}$ ) refers to the power line interference at 50 Hz, which was calculated by a 50 Hz second-order IIR peak filter. And the threshold was set at  $median(X_{LN-all} + 10 \times mad(X_{LN-all}))$ , where  $X_{LN-all}$  was the combined filtered signal of all channels for each subject,  $mad()$  was the mean absolute deviation. Channels whose LN ( $mean(X_{LN}^2)$ ) surpassed the threshold were removed. For the remaining channels, we applied a 4th order Butterworth filter to high-pass the signals at 0.5 Hz. Additionally, we utilized a notch filter to eliminate interferences caused by the signal at 50 Hz and its harmonics. To reduce motion artifacts, participants were seated semi-recumbent throughout the task, minimizing movement. Given the fixed placement of SEEG electrodes and the stationary nature of the setup,

no significant motion artifacts were observed during the initial visual inspection. Consequently, no specific motion artifact removal techniques were applied in subsequent analyses. The SEEG signal was segmented into 4000 ms epochs, including a 2500 ms pre-target cue and a 1500 ms time window after target onset.

### Frequency band segmentation and implications

In this study, we investigated neural synchronization across a broad spectrum of frequencies (1–140 Hz) to capture the diverse oscillatory dynamics associated with social interaction. Lower frequency was defined as below 30 Hz, while higher frequency was designated as gamma bands (30–140 Hz). For specific frequency band results interpretation, further subdivisions were employed: delta (1–4 Hz), theta (4–8 Hz), alpha (8–13 Hz), beta (13–30 Hz), low-gamma (30–45 Hz), middle-gamma (45–70 Hz), and high-gamma (70–140 Hz).<sup>87</sup> In line with previous literature,<sup>88</sup> our high-gamma frequency activity (HFA) measurements captured activity within the 70–140 Hz range. In the context of ESC, our focus lies on the interactions between lower frequency (1–30 Hz) oscillations and higher frequency (30–140 Hz) activity. PSI analyses guided by the intra-brain synchronization results and findings, concentrated on directed interactions within the 40 Hz range.

### Time-frequency analysis

We used wavelet transform to perform a time-frequency analysis of segmented signals in the insula and IFG.<sup>89</sup> For each trial, we applied a complex Morlet wavelet (6 cycles) convolution to the signal, to obtain power information across frequencies ranging from 1 to 140 Hz with a step size of 1 Hz.<sup>90</sup> The time-frequency power was then normalized by using mean and *SD* of the baseline (400 ms, –1900 ms ~ –1500 ms) per electrode and frequency. The baseline period was defined as the blank screen period (no visual stimulation), following the approach used in Barraza et al.'s study.<sup>66</sup>

### High-gamma frequency activity

We measured high-gamma frequency activity (HFA) with high frequency broadband amplitude (HFBA), which was used as a key electrophysiological marker of cortical electrical activity in previous studies.<sup>88,91</sup> In our study, HFBA was defined by a 70–140 Hz bandpass range. The preprocessed time series were filtered between 70 and 140 Hz using a sequential band-pass window of 10 Hz (i.e., 70–80, 80–90, 90–100 ... 130–140), via an FIR filter (Function *pop\_eegfiltnew* from EEGLAB toolbox). The amplitude (envelope) of each narrow band signal is then calculated by the Hilbert transform. The signal is then divided into 4000 ms epochs using the method mentioned above. Each narrow band time series was expressed as a percentage change from a baseline of 400ms (–1900ms ~ –1500ms) and averaged.

### Electrode selection

In line with previous studies,<sup>88,90,92</sup> we selected one representative electrode for each region of interest (ROI, i.e., insula and IFG) per participant to minimize inter-subject variability. We selected the most representative electrodes with reference to previous work.<sup>93</sup> Specifically, we first identified electrodes located within the ROIs based on electrode localization results. Next, we selected the most representative electrodes guided by HFBA. To address multiple comparison issues, statistical tests were performed using permutation tests based on non-parametric clustering. We tested whether HFBA during task ( $t = [0\ 1000]$  ms) differed significantly from baseline ( $t = [-1900\ -1500]$  ms). A reference distribution was generated by randomly shuffling data under the two conditions (task and baseline) and recalculating the test statistic 10000 times to assess the statistical significance of the actual data. Ultimately, 1–3 electrodes per brain region per participant met the statistical criteria ( $p < 0.05$ ). For participants with only one electrode meeting the criteria, we directly selected that electrode; for participants with multiple electrodes meeting the criteria, we invited experienced epileptologists to reconfirm and select one as the representative for the ROI.

### Intra-brain phase synchrony

To quantify the strength of neural synchronization between intra-brain regions, we used the weighted phase lag index (wPLI) metric. wPLI is a measure of functional connectivity that is only based on the imaginary component of the cross-spectrum. It has been shown to be less sensitive to volume conduction driven by single or common sources, and to additional irrelevant noise sources.<sup>54</sup> It is defined by the following formula:

$$wPLI = \frac{\text{abs}\left(\sum_{n=1}^{N_{trs}} \Im(X_{ij})\right)}{\sum_{n=1}^{N_{trs}} \text{abs}(\Im(X_{ij}))}$$

Where  $\Im(X_{ij})$  is the imaginary component of the cross-spectrum between channels  $i$  and  $j$  in the trial  $n$ , and  $N_{trs}$  is the number of trials. For each participant, we computed the wPLI between their intra-brain insula and IFG using the function (*ft\_connectivity\_wpli*) from the FieldTrip toolbox. To assess the significance level of the wPLI, we conducted a cluster-based permutation test. We randomly shuffled the signals of each electrode pair, calculated the corresponding wPLI, and repeated this process 1000 times, creating 1000 null distributions for each participant, as described in previous literature.<sup>77</sup> Subsequently, we employed cluster-based corrections for

multiple comparisons to obtain significant wPLI clusters ( $p < 0.05$ ). P-values were converted to z-scores, and z-maps were generated, where warmer colors indicate lower  $p$ -values.

### Envelope-to-signal coupling

To explore the relationship between lower frequency oscillations and higher frequency oscillations across brain regions, we used envelope-to-signal coupling (ESC) to measure this cross-frequency oscillation.<sup>56</sup> We estimated the ESC for all trials across participants inspired by the method described in the previous study.<sup>94</sup> First, to obtain the 1–30 Hz and 30–140 Hz components, SEEG signals were bandpass filtered around the center frequencies of 1–30 Hz with a step size of 1 Hz and 30 to 140 Hz in a step of 2 Hz. Then, the instantaneous amplitudes were extracted for each component within 30–140 Hz. ESC was calculated by correlating the envelopes of 30–140 Hz with the signals of 1–30 Hz and was averaged across trials. To avoid potential false positives, we created 1000 null distributions by randomly shuffling the signals of each trial in the two brain regions to obtain the null ESCs. Finally, we averaged the obtained null distributions and compared the observed mean ESC with the mean null distribution. The results only retained the values that exceeded 95% of the surrogate data.

### Phase slope index

Phase slope index (PSI) is a measure to estimate the direction of information flow between two time series.<sup>57</sup> In this study, we used PSI to estimate whether the slope of the phase difference between the insula and IFG signals is consistent over several adjacent frequency bins. If the PSI value is positive, it indicates that the insula signal leads the IFG signal, which is believed to be the flow from the insula to the IFG; a negative PSI indicates the reverse.<sup>95</sup> We calculated the PSI for the ipsilateral electrode pair (one insula channel and one IFG channel) of each participant using the function (*ft\_connectivityanalysis*) in the FieldTrip toolbox. To account for potential false positives, we followed the methods of previous studies to create 1000 null distributions and calculate the average null PSI.<sup>90,95</sup> The raw PSI was compared to the null PSI to calculate a Z score. A significant PSI was defined as  $|z| > 1.96$ , with  $z > 1.96$  indicating the insula as the leading region and  $z < -1.96$  indicating the IFG as the leading region.

### Granger causality

To further evaluate the potential causal relationships between the insula and IFG, we estimated Granger causality (GC). GC is a statistical method for assessing the conditional (asymmetric) dependence between two time series by investigating whether one time series can be used to correctly predict another time series.<sup>96,97</sup> As in the previous study,<sup>88</sup> we employed the MVGC toolbox<sup>98</sup> to compute spectral GC, describing the directional dependencies between the insula and IFG at different frequency bands. The model order was determined based on the Akaike information criterion, ranging from 6 to 10. To assess the significance of causal relationships, we conducted 1,000 permutation tests, with the permutation statistics computed by random shuffling of the time series. Significant causality was defined as exceeding the 99.9% confidence interval created by the permutation tests. Finally, we averaged the GC spectral curves across all participants to obtain the final causality estimates.

### Inter-brain coherence

We used the wPLI mentioned previously in intra-brain phase synchrony to evaluate the synchronization between the insula and the IFG of each pair of participants. For each pair of dyads, we computed the wPLI between ipsilateral insulas (e.g., the left insula of participant 1 and the left insula of participant 2) and IFGs. To assess the significance level of the wPLI, we conducted a cluster-based permutation test as described in the intra-brain phase synchrony section. We converted  $p$ -values to z-values and generated z-maps, with warmer colors indicating greater significance.

In this study, we conducted a detailed comparison of the wPLI values across various frequency bands during competitive and cooperative tasks. Our primary objective was to compare any significant differences in wPLI values ( $p < 0.05$ ) between the two conditions, encompassing the entire 1–140 Hz frequency range as well as the seven sub-bands (see [frequency band segmentation and implications](#)). To evaluate significant differences between cooperation (0–600 ms) and competition (0–300 ms) tasks, we employed the Wilcoxon rank-sum test. This non-parametric test was chosen for its effectiveness in comparing two independent samples of unequal sizes and distributions, providing a robust analysis of our data. To quantify the magnitude of synchrony differences observed between the two tasks, we calculated the median wPLI values for the entire 1–140 Hz and for each sub-band.

## QUANTIFICATION AND STATISTICAL ANALYSIS

Behavioral data were analyzed using MATLAB (R2021a, the MathWorks, Natick, MA, USA) and IBM SPSS version 22 (see [key resources table](#)). MATLAB was employed to calculate the mean and SD of RTs for each participant ( $n = 15$ ) in both tasks. Mann-Whitney U tests, conducted in SPSS, were used to compare RT and  $\Delta$ RT between 7 pairs of participants across the two tasks (see [behavioral results](#)).

All statistical analyses of SEEG data were performed using MATLAB and its associated toolboxes (see [method details](#) and [key resources table](#)). All tests were two-sided, with a significance level of 0.05 (\* represents  $p < 0.05$ , \*\* represents  $p < 0.01$ , \*\*\* represents  $p < 0.001$ ).

For HFBA, Spearman correlation was used to assess the correlation between mean responses in the insula and IFG across trials during the two tasks (see [results](#)). Independent samples t-tests were used to compare the HFBA between left and right hemispheres (see [Table S5](#)) and HFBA differences between two blocks within each task (See [Figure S1D](#) and its legend).

For intra-brain wPLI, Wilcoxon rank-sum tests were used to compare insula-IFG synchrony between the two tasks in 15 participants (see [results](#) and [Table S4](#)). For PSI, a null distribution was generated using 1000 permutations to determine the significance threshold. Z-scores were calculated by comparing the raw PSI with the null PSI, using a 95% confidence interval (see [results](#), [Figure 3](#) and its legend). For Granger causality, a significance threshold was determined based on the 99.9% confidence interval from 1000 permutations. Results are presented as mean and SEM of GC across 15 participants (see [results](#), [Figure S2](#) and its legend).

For inter-brain wPLI, Wilcoxon rank-sum tests were used to compare synchrony between inter-brain regions (insula-insula; IFG-IFG) in 7 pairs of participants across the two tasks (see [results](#), [Tables 2](#) and [3](#)). Cluster-based permutation tests with 2000 permutations were used to examine temporal differences in inter-brain synchronization between the two blocks (see [Figure S1E](#)).